2012

Accessibility and Selective Stabilization of the Principal Spin States of Iron by Pyridyl versus Phenolic Ketimines: Modulation of the $^6A1 \leftrightarrow {}^2T_2$ Ground-State Transformation of the $[FeN_4O_2]+$ Chromophore

Musa S. Shongwe
Sultan Qaboos University

Usama A. Al-Zaabi
Sultan Qaboos University

Faizah Al-Mjeni
Sultan Qaboos University

Carla S. Eribal
Western Michigan University

Imaddin A. Al-Omari
Sultan Qaboos University

See next page for additional authors

Published in *Inorganic Chemistry* 51:15 (2012), pp. 8241−8253; doi: 10.1021/ic300732r

Submitted April 16, 2012; published online July 18, 2012.

The authors declare no competing financial interest.

Supporting information for this article is available following the references.

Accessibility and Selective Stabilization of the Principal Spin States of Iron by Pyridyl versus Phenolic Ketimines: Modulation of the $^6A_1 \leftrightarrow {}^2T_2$ Ground-State Transformation of the $[FeN_4O_2]^+$ Chromophore

Musa S. Shongwe,[1] Usama A. Al-Zaabi,[1] Faizah Al-Mjeni,[1] Carla S. Eribal,[2] Ekkehard Sinn,[2] Imaddin A. Al-Omari,[3] Hussein H. Hamdeh,[4] Dariusz Matoga,[5] Harry Adams,[6] Michael J. Morris,[6] Arnold L. Rheingold,[7] Eckhard Bill,[8] and David J. Sellmyer[9]

1. Department of Chemistry, College of Science, Sultan Qaboos University, PO Box 36, Al-Khod 123, Muscat, Sultanate of Oman
2. Department of Chemistry, Western Michigan University, Kalamazoo, Michigan 49008, United States
3. Department of Physics, College of Science, Sultan Qaboos University, PO Box 36, Al-Khod 123, Muscat, Sultanate of Oman
4. Department of Physics, Wichita State University, 1845 Fairmount St, Wichita, Kansas 67260, United States
5. Faculty of Chemistry, Jagiellonian University, Ingardena 3, 30-060 Kraków, Poland
6. Department of Chemistry, University of Sheffield, Sheffield S3 7HF, UK
7. Department of Chemistry and Biochemistry, University of California, San Diego, La Jolla, California 92093-0358, United States
8. Max-Planck-Institut für Bioanorganische Chemie, Stiftstrasse 34-36, 45470 Mülheim an der Ruhr, Germany
9. Department of Physics and Astronomy and Nebraska Center for Materials and Nanoscience, University of Nebraska–Lincoln, Nebraska 68588, United States

Corresponding author – Musa S. Shongwe, email musa@squ.edu.om

Abstract

Several potentially tridentate pyridyl and phenolic Schiff bases (apRen and HhapRen, respectively) were derived from the condensation reactions of 2-acetylpyridine (ap) and 2′-hydroxyacetophenone (Hhap), respectively, with N-R-ethylenediamine ($RNHCH_2CH_2NH_2$, Ren; R = H, Me or Et) and complexed in situ with iron(II) or iron(III), as dictated by the nature of the ligand donor set, to generate the six-coordinate iron compounds $[Fe^{II}(apRen)_2]X_2$ (R = H, Me; X^- = ClO_4^-, BPh_4^-, PF_6^-) and $[Fe^{III}(hapRen)_2]X$ (R = Me, Et; X^- = ClO_4^-, BPh_4^-). Single-crystal X-ray analyses of $[Fe^{II}(apRen)_2](ClO_4)_2$ (R = H, Me) revealed a pseudo-octahedral geometry about the ferrous ion with the Fe^{II}–N bond distances (1.896–2.041 Å) pointing to the $^1A_1$ ($d\pi^6$) ground state; the existence of this spin state was corroborated by magnetic susceptibility measurements and Mössbauer spectroscopy. In contrast, the X-ray structure of the phenolate complex $[Fe^{III}(hapMen)_2]ClO_4$, determined at 100 K, demonstrated stabilization of the ferric state; the compression of the coordinate bonds at the metal center is in accord with the $^2T_2$ ($d\pi^5$) ground state. Magnetic susceptibility measurements along with EPR and Mössbauer spectroscopic techniques have shown that the iron(III) complexes are spin-crossover (SCO) materials. The spin transition within the $[Fe^{III}N_4O_2]^+$ chromophore was modulated with alkyl substituents to afford two-step and one-step $^6A_1 \leftrightarrow {}^2T_2$ transformations in $[Fe^{III}(hapMen)_2]ClO_4$ and $[Fe^{III}(hapEen)_2]ClO_4$, respectively. Previously, none of the X-salRen- and Xsal2trien-based ferric spin-crossover compounds exhibited a stepwise transition. The optical spectra of the LS iron(II) and SCO iron(III) complexes display intense $d\pi \rightarrow p\pi^*$ and $p\pi \rightarrow d\pi$ CT visible absorptions, respectively, which account for the spectacular color differences. All the complexes are redox-active; as expected, the one-electron oxidative process in the divalent compounds occurs at higher redox potentials than does the reverse process in the trivalent compounds. The cyclic voltammograms of the latter compounds reveal irreversible electrochemical generation of the phenoxyl radical. Finally, the H_2salen-type quadridentate ketimine H_2hapen complexed with an equivalent amount of iron(III) to afford the μ-oxo-monobridged dinuclear complex $[\{Fe^{III}(hapen)\}_2(\mu\text{-}O)]$ exhibiting a distorted square-pyramidal geometry at the metal centers and considerable antiferromagnetic coupling of spins ($J \approx -99\ cm^{-1}$).

Introduction

The ease with which iron exhibits multiple oxidation states and an array of accessible spin states (S = 0–5/2) is held in some measure responsible for the richness of the coordination chemistry of this bioactive metal.[1,2] The spin-crossover phenomenon was first recognized in iron-based dithiocarbamato complexes eight decades ago.[3] Since then spin crossover has been observed in complexes of other transition metals that meet the basic criteria in terms of the ground-state electron configuration of the metal center (d^4–d^7, octahedral) and the ligand-field strength ($P \approx \Delta_o$), notably manganese(III)[4] and cobalt(II)[5] complexes. Spin crossover is of immense fundamental and technological interest with applications envisaged in the fabrication of molecule-based electronic devices for visual displays and information storage.

Spin crossover is by far more prevalent for iron(II)[6,7] than for iron(III),[7,8] whereas there is rapid development of ferrous spin crossover borne out by the ever-increasing research output on such iron(II) SCO materials, there are only a mere handful of examples of ferric spin-crossover compounds reported in recent times. A preponderance of iron(II) spin-crossover substances possess the $[FeN_6]^{2+}$ coordination sphere;[6] however, there is a growing number of examples of ferrous spin-crossover complexes supported by an $[N_4O_2]$ donor set.[9] In contrast, the vast majority of iron(III) spin transitions occur within the $[FeN_4O_2]$ core[8] with the oxygen atoms mostly phenolic in nature; ferric spin-crossover materials featuring an all-N-donor environment are extremely rare.[10]

Exposure of SCO molecular materials to external perturbations, such as temperature, pressure, or electromagnetic radiation, induces a variety of spin transitions,[6−10] namely, abrupt, gradual, complete, incomplete (at either or both ends of the spin-transition curve), one-step, two-step one-sited, twostep two-sited, symmetry-breaking and hysteretic, as well as various combinations of some of these. It is now well established that strong cooperativity of spin-crossover centers in the crystal lattice causes abrupt reversible spin transitions with a relatively large thermal hysteresis loop, a property highly desired for applications in molecular electronics.[7] Such cooperativity tends to arise from intermolecular forces including hydrogen bonding and $\pi-\pi$ stacking interactions. Spin transitions are influenced by several factors,[6−10] including ligand substituent groups (steric and electronic effects), solvents of crystallization, counterions, sample type and, in rare cases, configurational isomerism.[11]

It is rather surprising that the seemingly attractive heterodonor apRen and HhapRen Schiff bases have received very little attention, some derivatives none at all, in coordination chemistry. The only literature report on the iron chemistry of apHen is the classic paper of Krumholz on MLCT spectra of low-spin iron(II)–imine complexes.[12] Only nickel(II)[13] and copper(II)[14] complexes with apHen have ever been structurally characterized. As far as we are aware, the coordination chemistry of apMen and the phenolic ligands HhapRen has never been explored previously. Of the analogous ferric phenolate SCO materials $[Fe^{III}(X\text{-}salRen)_2]Y$[15] and $[Fe^{III}(X\text{-}sal)_2trien]Y$[16] only a few exhibited abrupt or hysteretic spin transitions; none displayed two-step $^6A_1 \leftrightarrow {}^2T_2$ transformations. In this work, the use of apMen and HhapMen sought to compare and contrast the iron-coordination properties of the pyridyl and phenolate moieties on an equal footing. The compounds $[Fe^{III}(hapEen)_2]ClO_4$, $[Fe^{III}(hapMen)_2]ClO_4$, and $[Fe^{III}(hapMen)_2]BPh_4$ were intended to tune the spin crossover in this ketimine system.

Results and Discussion

Synthetic Routes, Chemical Formulations, and Spectroscopic Identification

The Schiff bases apRen (R = H, Me) and HhapRen (R = Me, Et) were generated by the condensation reaction of stoichiometric amounts of either 2-acetylpyridine or 2′-hydroxyacetophenone (a ketone), respectively, with the appropriate primary amine (*N*-R-ethylenediamine) in refluxing MeOH or EtOH (scheme 1).

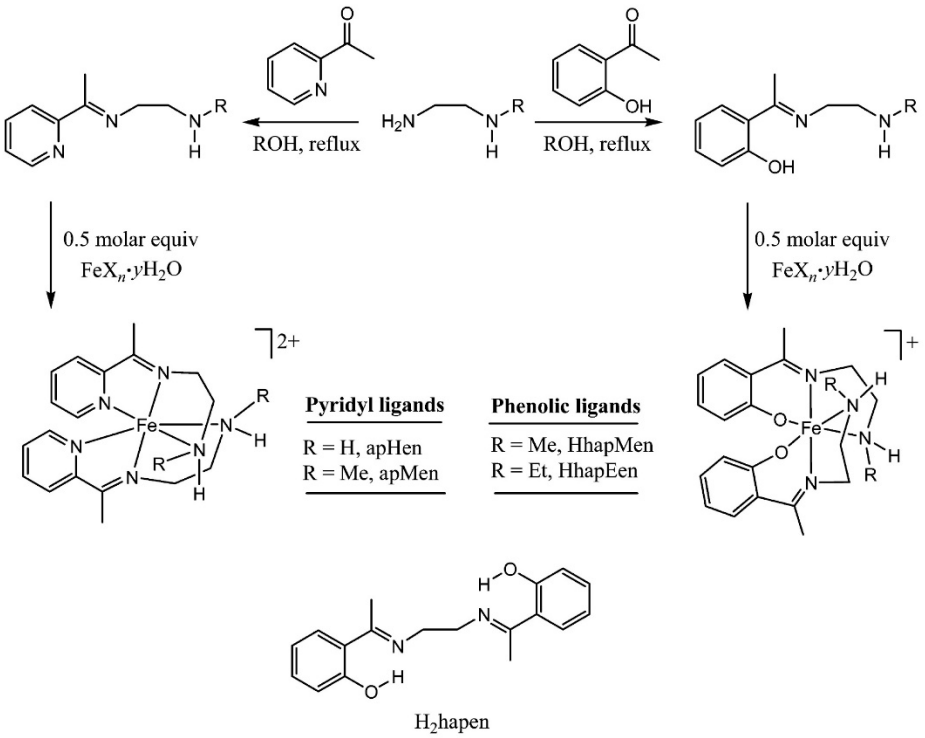

Scheme 1. Synthetic Pathways and Ligand Designations

With the exception of H$_2$hapen, these ligands were not isolated as solids but rather were complexed in situ with iron(II) or iron(III) to afford the desired iron compounds. However, for spectroscopic characterization, the solutions of HhapRen and apRen were stripped of the solvent to give viscous orange liquids. The chemical identity of H$_2$hapen, a potentially quadridentate Schiff-base ligand, was established by microanalysis (C, H, and N) and EI mass spectrometry. Its characteristic functional features, namely, azomethine C=N and phenolic OH groups, were readily identified by their vibrational stretches at 1611 and 3450 cm^{-1}, respectively. The ^{1}H NMR spectra of the ligands (see Supporting Information) are comparable with those of closely related Schiff bases.[17] That of H$_2$hapen is displayed in Supporting Information figure S1. The signature color of the Schiff bases appears to originate from $\pi \rightarrow \pi^*$ electronic transitions occurring within the imine bonds; this assertion is supported by the observation that reduction of these ligands with NaBH$_4$ in refluxing EtOH causes disappearance of both the color and the visible (or near-visible) absorption band. This spectroscopic feature of the ligands is exemplified by HhapMen in Supporting Information figure S2.

The iron(II)−pyridyl compounds [Fe^{II}(apHen)$_2$]X$_2$ and [Fe^{II}(apMen)$_2$]X$_2$ (X = ClO$_4^-$, BPh$_4^-$, or PF$_6^-$) were synthesized by reaction of the appropriate Schiff base produced in situ with half molar equivalent of iron(II) or iron(III) ion. That these all-N-donor ligands have a preference for iron(II) over iron(III) has been demonstrated by their reaction with the latter which resulted in spontaneous reduction to the ferrous ion. The varying of the counterions was motivated principally by the quest to probe the effect of counterions on iron spin crossover.[18] On going from apHen to apMen, there occur discernible color differences between

the complex cations $[Fe^{II}(apHen)_2]^{2+}$ (navy-blue) and $[Fe^{II}(apMen)_2]^{2+}$ (purple-tinged royal blue).

The iron(III)−phenolate compounds $[Fe(hapMen)_2]X$ ($X^- = ClO_4^-$ or BPh_4^-) and $Fe(hapEen)_2]ClO_4$ were produced from the reactions of stoichiometric amounts of HhapRen (R = Me or Et) with Fe^{II} or Fe^{III} ion as described for the analogous aforementioned iron(II)−pyridyl complexes, but in this case the iron(II) was spontaneously oxidized to iron(III), indicating that the donor set N_4O_2 stabilizes the ferric state preferentially. These iron(III)−phenolate complexes are purple-pink or violet in solution. The complex of the quadridentate Schiff-base ligand H_2hapen with iron(III), $[\{Fe(hapen)\}_2(\mu\text{-}O)]$, was synthesized by reaction of the ligand (produced in situ or isolated as crystals) with $Fe(ClO_4)_2{\cdot}xH_2O$ or $Fe(ClO_4)_3{\cdot}xH_2O$ as the source of the iron.

The chemical formulations of the iron(II) complexes $[Fe(apRen)_2]X_2$ (R = H, Me; $X^- = ClO_4^-$, PF_6^-), $[Fe(apHen)_2](BPh_4)_2{\cdot}2H_2O$, and $[Fe(apMen)_2](BPh_4)_2{\cdot}4H_2O$, as well as the iron(III) complexes $[Fe(hapMen)_2]X$ ($X^- = ClO_4^-$, BPh_4^-) and $[Fe(hapEen)_2]ClO_4$, were verified by elemental analyses (C, H, and N) and FAB mass spectrometry. Supporting Information figure S3 illustrates the mass spectral characterization of the iron(II) and iron(III) bis-chelate complexes and reveals an interesting difference between the pyridyl and phenolate complexes. The FAB mass spectrum of $[Fe(apHen)_2](ClO_4)_2$ [Supporting Information figure S3a] in the positive mode displays peaks at m/z = 382 and 218 representing the complex cation $[Fe(apHen)_2]^{2+}$ and the fragment "$[Fe(apHen)]^{2+}$", respectively. Surprisingly, there is an additional peak at m/z = 481 corresponding to the formula unit "$[Fe(apHen)_2]ClO_4$", which indicates retention of one of the perchlorate counterions. In contrast, this behavior is not observed in the case of the iron(III)−phenolate complexes as illustrated by the FAB mass spectrum of $[Fe(hapMen)_2]ClO_4$ [Supporting Information figure S3b], which exhibits a molecular peak for the complex cation at m/z = 438 and reveals dissociation of one ligand to give the fragment "$[Fe(hapMen)]^{2+}$". Finally, according to mass spectrometry, the dinuclear iron(III) complex $[\{Fe(hapen)\}_2(\mu\text{-}O)]$ ruptures asymmetrically at the μ-oxo bridge to give the structural units "[Fe(hapen)(O)]" (m/z = 366) and "[Fe(hapen)]" (m/z = 350). This bridge breakage is reminiscent of that which was observed in the vanadium(IV) thiosemicarbazonato dimer $[\{V(daptsc)(MeOH)\}_2(\mu\text{-}O)](ClO_4)_2$.[19]

In the IR spectra of the iron compounds, the vibrational bands of importance that stand out are those of the azomethine bond, the amino group, the aromatic ring, and the counterions. The ν(C=N) vibrations occurring typically in the range 1596−1601 cm^{-1} verified the existence of the Schiff-base ligands in these complexes. The amino groups exhibit ν(N−H) absorptions between 3100 and 3400 cm^{-1} whereas the pyridyl and phenolate ring vibrations are the dominant features in the region 1400−1590 cm^{-1}. As for the iron−phenolate complexes, prominent absorption bands associated with ν(C−O), conspicuously absent from the spectra of the iron−pyridyl complexes, are observed between 1200 and 1300 cm^{-1}. The spectrum of the dinuclear complex $[\{Fe(hapen)\}_2(\mu\text{-}O)]$ reveals stretches at 842 and 422 cm^{-1} consistent with ν_{as}(Fe−O_{oxo}) and ν_s(Fe−O_{oxo}), respectively, of the angular bridge $[Fe{-}O{-}Fe]^{4+}$. For closely related μ-oxo-monobridged diiron(III) complexes, the asymmetric stretch lies typically in the range 730−880 cm^{-1}, whereas the symmetric vibration occurs between 360 and 545 cm^{-1}; the latter is forbidden in the IR region for linear [Fe−O−Fe] cores.[1b,c] Each counterion presents a unique and conspicuous feature at the lower-energy end of the spectrum. Generally, $\nu(ClO_4^-)$[8a,b] gives rise to strong absorptions around 1145, 1120, and 1090 cm^{-1} along with a relatively weaker one at ~625 cm^{-1}. The tetraphenylborate ion[16a,20] is char-

acterized by intense vibrational bands in the ranges 730−740 and 700−710 cm^{-1} accompanied by an absorption band of medium intensity between 610 and 615 cm^{-1}. The stretches of the PF_6^- ion[16a] are readily recognizable by their characteristic absorptions at 842 (s) and 558 (m) cm^{-1}.

Elucidation of Molecular Structures

The 3-D structures of $[Fe(apHen)_2](ClO_4)_2$, $[Fe(apMen)_2](ClO_4)_2$, $[Fe(hapMen)_2](ClO_4)_2$, H_2hapen, and $[\{Fe(hapen)\}_2(\mu\text{-}O)]$ have been determined by single-crystal X-ray crystallography. Blocks of $[Fe(apHen)_2](ClO_4)_2$ and $[Fe(apMen)_2](ClO_4)_2$ amenable to single-crystal X-ray analyses were grown from methanol solutions of these iron compounds by slow evaporation of the solvent. Both compounds crystallized in the monoclinic space group $P2_1/c$. A summary of the crystallographic data is provided in table 1. As expected, $[Fe(apHen)_2](ClO_4)_2$ and $[Fe(apMen)_2](ClO_4)_2$ are isostructural and possess comparable crystallographic parameters. Each crystal structure is composed of a mononuclear $[Fe(apRen)_2]^{2+}$ (R = H or Me) complex cation and two disordered perchlorate counterions. In the case of $[Fe(apMen)_2](ClO_4)_2$, these counterions were eliminated using the PLATON SQUEEZE function[21] as indicated in the relevant CIF. The X-ray analyses gave definitive evidence for the stabilization of the divalent state of iron by the pyridyl ketimines. Figures 1 and 2 depict the X-ray structures of the complex cations $[Fe(apHen)_2]^{2+}$ and $[Fe(apMen)_2]^{2+}$, respectively, with selected pertinent bond distances and angles compiled in table 2. In each structure, the iron(II) ion is in a distorted octahedral environment created by the two tridentate apRen ligands which are oriented nearly orthogonally to each other. Each apRen ligand provides three types of nitrogen donor atoms for coordination, namely, pyridyl, imine, and amine. As is often the case with tridentate Schiff bases, the apRen ligand is oriented such that each donor set adopts a meridional arrangement with the imine nitrogens occupying trans positions relative to each other. In $[Fe(apHen)_2](ClO_4)_2$, the cis angles range from 80.47(13)° to 99.94(12)°, and the trans ones are 164.21(12)°, 164.29(13)°, and 179.30(13)°; these compare favorably with those of the [Fe(apMen)2](ClO4)2 congener [cis angles = 80.40(11)− 98.61(11)°; trans angles = 163.26(12)°, 164.20(11)°, and 178.36(11)°].

Table 1. Selected Crystallographic Data for H2hapen, $[Fe^{II}(apRen)_2](ClO_4)_2$ (R = H, Me), $[Fe^{III}(hapMen)_2]ClO_4$, and $[\{Fe^{III}(hapen)\}_2(\mu\text{-}O)]$

	H2hapen	$[Fe(apHen)_2](ClO_4)_2$	$[Fe(apMen)_2](ClO_4)_2$	$[Fe(hapMen)_2]ClO_4$	$[\{Fe^{III}(hapen)\}_2(\mu\text{-}O)]$
empirical formula	$C_{18}H_{20}N_2O_2$	$C_{18}H_{26}N_6O_8Cl_2Fe$	$C_{20}H_{30}N_6O_8Cl_2Fe$	$C_{22}H_{30}N_4O_6ClFe$	$C_{36}H_{36}N_4O_5Fe$
molar mass (g/mol)	296.36	581.20	609.25	537.80	716.39
T (K)	150	150	208	100	100
crystal system	monoclinic	monoclinic	monoclinic	monoclinic	triclinic
space group	$P2_1/n$	$P2_1/c$	$P2_1/c$	$P2_1/c$	$P\bar{1}$
a (Å)	5.6177(2)	15.7479(19)	16.3596(18)	8.0933(8)	11.500(4)
b (Å)	20.4136(8)	9.8664(12)	10.4130(12)	8.6263(8)	11.623(4)
c (Å)	6.7833(3)	15.2144(18)	15.3533(17)	33.904(3)	14.007(4)
α (deg)	90	90	90	90	81.618(4)
β (deg)	104.412(3)	95.654(2)	97.8400(10)	90.7700(10)	73.509(4)
γ (deg)	90	90	90	90	61.073(3)
V (Å^3)	753.41(5)	2352.4(5)	2591.0(5)	2366.8(4)	1571.2(8)
Z	2	4	4	4	2
ρ_{calcd} (g/cm^3)	1.306	1.641	1.557	1.504	1.514
μ (mm^{-1})	0.086	0.926	0.845	0.796	0.975
F(000)	316	1200	1256	1116	744
crystal size (mm)	0.26 × 0.24 × 0.09	0.34 × 0.32 × 0.21	0.40 × 0.40 × 0.32	0.41 × 0.38 × 0.34	0.28 × 0.22 × 0.17
θ range (deg)	2.00–36.53	1.30–28.59	1.26–25.93	2.40–25.40	1.52–25.00
reflns collected	15 539	26 199	23 732	13 623	26 214
independent reflns	3699	5611	4972	4337	5532
R_{int}	0.0263	0.0705	0.0597	0.0275	0.0990
GOF on F^2	0.998	1.020	1.073	1.008	1.071
R_1, R_2 [$I > 2\sigma(I)$]	0.0487, 0.1331	0.0553, 0.1360	0.0555, 0.1293	0.0365, 0.0983	0.0690, 0.1696
R_1, R_2 (all data)	0.0677, 0.1463	0.0969, 0.1527	0.0774, 0.1380	0.0415, 0.1014	0.1111, 0.1925

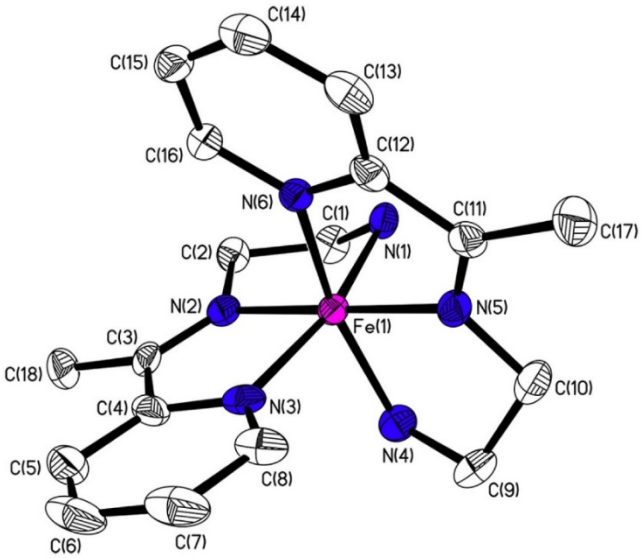

Figure 1. X-ray structure of the complex cation in $[Fe(apHen)_2](ClO_4)_2$.

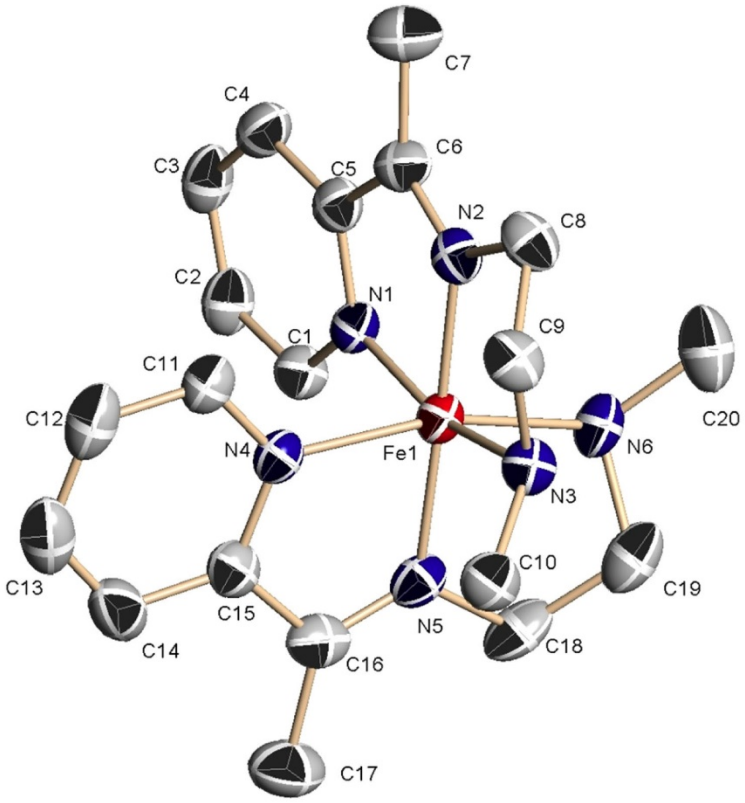

Figure 2. X-ray structure of the complex cation in $[Fe(apMen)_2](ClO_4)_2$.

Table 2. Selected Bond Distances (Å) and Angles (deg) for $[Fe^{II}(apHen)_2](ClO_4)_2$, $[Fe^{II}(apMen)_2](ClO_4)_2$, and $[Fe^{III}(hapMen)_2]ClO_4$

$[Fe^{II}(apHen)_2](ClO_4)_2$		$[Fe^{II}(apMen)_2](ClO_4)_2$		$[Fe^{III}(hapMen)_2]ClO_4$	
Fe(1)–N(5)	1.897(3)	Fe(1)–N(2)	1.896(3)	Fe(1)–O(1)	1.8649(16)
Fe(1)–N(2)	1.901(3)	Fe(1)–N(5)	1.902(3)	Fe(1)–O(2)	1.8652(16)
Fe(1)–N(3)	1.952(3)	Fe(1)–N(4)	1.959(3)	Fe(1)–N(1)	1.9397(19)
Fe(1)–N(6)	1.958(3)	Fe(1)–N(1)	1.964(2)	Fe(1)–N(3)	1.9405(19)
Fe(1)–N(4)	2.019(3)	Fe(1)–N(6)	2.041(3)	Fe(1)–N(4)	2.048(2)
Fe(1)–N(1)	2.024(3)	Fe(1)–N(3)	2.041(3)	Fe(1)–N(2)	2.050(2)
C(3)–N(2)	1.296(5)	C(6)–N(2)	1.292(4)	C(7)–N(1)	1.292(3)
C(2)–N(2)	1.470(4)	C(8)–N(2)	1.462(4)	C(9)–N(1)	1.472(3)
C(11)–N(5)	1.291(5)	C(16)–N(5)	1.290(4)	C(18)–N(3)	1.298(3)
C(10)–N(5)	1.466(5)	C(18)–N(5)	1.470(4)	C(20)–N(3)	1.478(3)
$\Sigma = 71.73°$[a]		$\Sigma = 72.73°$[a]		$\Sigma = 29.74°$[a]	
N(5)–Fe(1)–N(2)	179.30(13)	N(2)–Fe(1)–N(5)	178.36(11)	N(1)–Fe(1)–N(3)	176.37(8)
N(6)–Fe(1)–N(4)	164.21(12)	N(4)–Fe(1)–N(6)	163.26(12)	O(2)–Fe(1)–N(4)	178.15(8)
N(3)–Fe(1)–N(1)	164.29(13)	N(1)–Fe(1)–N(3)	164.20(11)	O(1)–Fe(1)–N(2)	176.26(7)

a. NB: Σ is the angular distortion parameter, which represents the sum of the deviations of the cis angles from the idealized angle.

The chelate angles formed by the pyridyl and imine nitrogens [80.47(13) and 81.07(13)°] in $[Fe(apHen)_2](ClO_4)_2$ and [80.40(11) and 80.57(11)°] in $[Fe(apMen)_2](ClO_4)_2$] are comparable with the bite angles observed in related low-spin pseudo-octahedral iron(II) Schiff-base complexes with the pyridyl-imine structural unit.[22] A direct comparison can be made between the $N_p–M–N_i$ [M = Fe^{2+} (LS) or Ni^{2+}] bite angles in $[Fe(apHen)_2]^{2+}$ and $[Ni(apHen)_2]^{2+}$:[13] the angles are significantly smaller for the latter complex cation [77.5(2)° and 77.8(2)°] because Ni^{2+} is larger than LS Fe^{2+} [ionic radii $r_{Fe(II)}$ = 75 pm, $r_{Ni(II)}$ = 83 pm). The $N_p–M–N_i$ chelate angle is a useful distinguishing feature between HS Fe^{II} and LS Fe^{II}. This geometric parameter typically falls within the range ~73–77° for the $^5T_2$ ground state.[22a,23] The average $Fe^{II}–N$ bond lengths 1.955 Å ($Fe^{II}–N_{pyridyl}$), 1.899 Å ($Fe^{II}–N_{imine}$) and 2.022 Å ($Fe^{II}–N_{amine}$) for $[Fe(apHen)_2](ClO_4)_2$, and 1.962 Å ($Fe^{II}–N_{pyridyl}$), 1.899 Å ($Fe^{II}–N_{imine}$), and 2.041 Å ($Fe^{II}–N_{amine}$) for $[Fe(apMen)_2](ClO_4)_2$ are in keeping with the low-spin state of the complex cations and are comparable with those of related low-spin iron(II) complexes.[18a,b,22–24] LS Fe^{II} is favored over HS Fe^{II} by the greater ligand-field stabilization energy (t_{2g}^6 vs $t_{2g}^4e_g^2$ configuration).

X-ray data collection on a single crystal of $[Fe(hapMen)_2]ClO_4$ was performed at 100 K. The crystal system and space group are identical to those of the corresponding pyridyl analogue, $[Fe(apMen)_2](ClO_4)_2$. Crystal data along with structure solution and refinement parameters for $[Fe(hapMen)_2]ClO_4$ are summarized in table 1. Selected bond distances and angles are given in table 2. The crystal structure of $[Fe(hapMen)_2]ClO_4$ consists of a mononuclear $[Fe(hapMen)_2]^+$ complex cation with a perchlorate counteranion, pointing to the trivalent state of the central metal atom. The structure of the complex cation is depicted in figure 3. Each of the two uninegative tridentate Schiff-base ligands provides a phenolate oxygen, an imine nitrogen and a secondary amine nitrogen as donor atoms to create a six-coordinate geometry about the iron(III) ion. The azomethine (C=N) bonds (average distance =1.295 Å) confer rigidity to the ligands and influence a meridional arrangement of the donor atoms with the imine nitrogen atoms of the two ligands oriented trans to each other [N(1)–Fe(1)–N(3) = 176.37(8)°]. Each of the other two pairs of trans bonds is $O_{phenolate}–Fe–N_{amine}$ [176.26(7)° and 178.15(8)°] from the same ligand. The phenolate moieties of the two ligands are adjacent to each other [O(1)–Fe(1)–O(2) = 91.59(7)°] as are the secondary amines [N(2)–Fe(1)–N(4) = 88.90(8)°]. Incidentally, recently, Verani et al.[25] demonstrated crystallographically that the rigidity or flexibility of the framework of a tridentate ligand and the nature of a substituent group dictate the geometric isomer (fac or mer) to be adopted by an octahedral complex. A ligand structural feature of interest in $[Fe(hapMen)_2]ClO_4$ is the extension of the delocalization of π-electrons to the phenolate oxygen atom as evidenced by the relatively short phenolate C–O bond [1.326(3) and 1.324(3) Å].

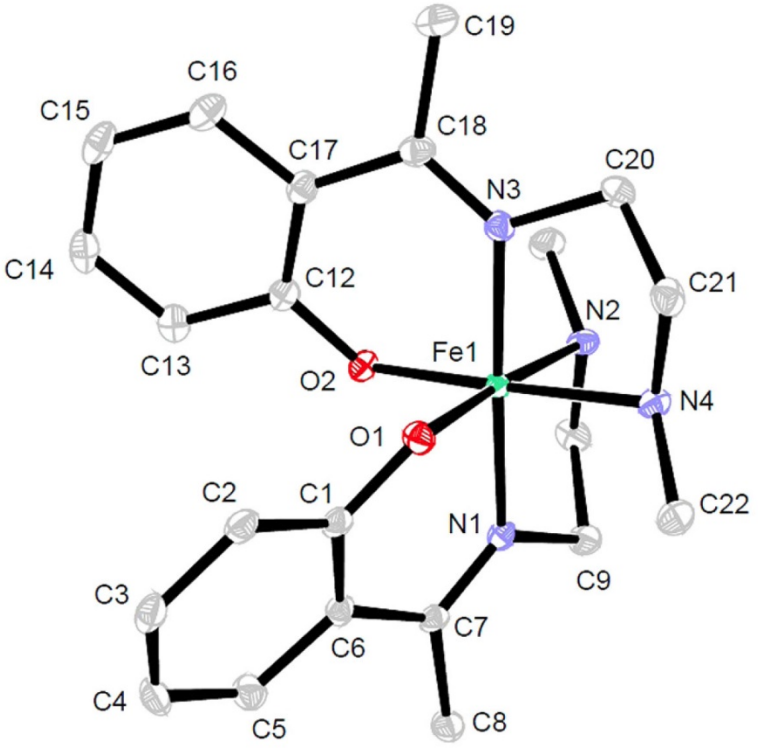

Figure 3. X-ray structure of the cation in $[Fe(hapMen)_2]ClO_4$.

The cis angles in the coordination sphere range from 84.84(8)° to 94.42(8)° with the octahedral angular distortion parameter, $\Sigma = 29.74°$ (the sum of the deviations of the cis angles from the idealized angle), indicative of the $^2T_2$ ground state. In the closely related salicylaldimine ferric complexes,[15a,f,h,i] the value of Σ lies approximately within the ranges 40–50° and 65–75° for the $^2T_2$ and $^6A_1$ ground states, respectively. Generally, the N_{im}–Fe^{III}–N_{am} bite angle of the 5-membered *en*-chelate ring is more reliable in predicting the spin state: HS, 78–80°; LS, 83–85°. For $[Fe(hapMen)_2]ClO_4$, this angular parameter has an average value of ~85.0° (LS). The average distances of the bonds Fe^{III}–$O_{phenolate}$ (1.8651 Å), Fe^{III}–N_{imine} (1.9401 Å) and Fe^{III}–N_{amine} (2.049 Å) are consistent with the low-spin state of iron(III) in a pseudooctahedral geometry. Typically, octahedral LS distances of Fe^{III}–$O_{phenolate}$, Fe^{III}–N_{imine}, and Fe^{III}–N_{amine} are in the ranges 1.85–1.89,[8,15,16,26] 1.92–1.96,[8,15,16,26] and 2.02–2.08 Å,[15,16,26a] respectively, whereas the corresponding distances for HS iron(III) are in the ranges 1.89–1.93,[8,15,16,26,27] 2.09– 2.15,[8,15,16,26] and 2.18–2.26 Å,[15,16,26a,27a] respectively. These variations of bond distances with spin state are readily explained using MO theory which shows an antibonding (d_σ*) HOMO in HS octahedral iron(III) complexes, but a nonbonding ($d\pi$) HOMO in the corresponding LS complexes. Alternatively, the disparity in the metal–ligand bond lengths upon spin conversion can be explained in terms of the variation of the ionic radius at the metal center. HS Fe^{III} in an octahedral field is expected to exhibit a larger ionic radius, hence longer Fe^{III}–L bonds, than the corresponding LS ferric ion.

The potentially quadridentate ligand H_2hapen crystallized in the monoclinic space group $P2_1/n$. The crystallographic data are compiled in table 1. A conspicuous feature of the molecular structure of H_2hapen (fig. 4) is the centrosymmetry with the inversion center located in the middle of the C–C bond of the ethylenediimine backbone. The enolimine

tautomeric form of this Schiff base is stabilized by the intramolecular hydrogen bonding $O(1)-H(1)_{phenolic}\cdots N(1)_{imine}$ [O(1)−H(1) = 0.84 Å, H(1)···N(1) = 1.90 Å, O(1)···N(1) = 2.5071(10) Å, O(1)−H(1)−N(1) = 128.2°]. H_2hapen is isostructural with the analogous Schiff-base ligand 2,2′-[(1,2-ethanediyl)bis-(nitrilopropylidyne)]bisphenol (H_2hppen).[28] However, the molecular structure of the analogue 2,2′-{(1,2-ethanediyl)bis[nitrilo(phenyl)methylidyne]}bisphenol (H_2hbpen)[28] exhibits a gauche conformation.

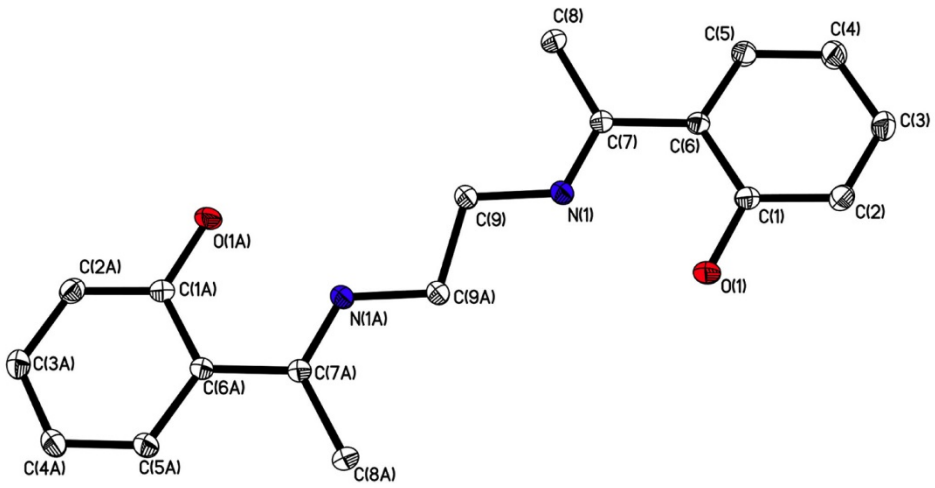

Figure 4. X-ray structure of H_2hapen.

[{Fe(hapen)}$_2$(μ-O)] crystallized in the triclinic *P*$\bar{1}$ space group. The crystallographic data for this complex are summarized in table 1 and selected geometric parameters are presented in Supporting Information table S1. The molecular structure of [{Fe(hapen)}$_2$(μ-O)] is depicted in figure 5. The structural feature that stands out is the μ-oxo-monobridged diiron(III), [Fe−O−Fe]$^{4+}$, core. The Fe−O−Fe bridge bond lengths Fe(1)−O(5) = 1.787(4) Å and Fe(2)−O(5) = 1.776(5) Å are consistent with high-spin iron(III) centers and lie in the literature range 1.73−1.82 Å for similar iron(III) dinuclear complexes.[2,29] The $Fe^{III}\cdots Fe^{III}$ separation (3.484 Å) compares favorably with the corresponding distances observed in related μ-oxo-monobridged dinuclear complexes of iron(III) (3.39−3.62 Å).[2,29] The bridge angle Fe(1)−O(5)−Fe(2) = 155.9(3)° is considerably bent. The corresponding angles in the structure of [{Fe(salen)}$_2$(μ-O)] from two independent crystallographic studies are 144.6°[29m] and 147.8°.[29n] Interestingly, for the complex [{Fe(3,5-^{t}Bu$_2$-salen)}$_2$(μ-O][29e] with the bulky *tert*-butyl substituent groups on the ligand framework, the Fe−O−Fe angle is 171.63(17)°. Sterically encumbering groups on salen-based ligands impose linearity on the Fe−O−Fe linkage.[29e] This bridge angle is somewhat larger in [{Fe(hapen)}$_2$(μ-O)] than in [{Fe(salen)}$_2$(μ-O)] possibly due to the presence of the azomethine methyl groups on the backbone of hapen^{2-}. In the recent work of Glaser et al.[29q] on μ-oxo-monobridged dinuclear iron(III) complexes with the variously substituted tetradentate ligand system *N*,*N*′-dimethyl-1,2- diaminoethane, the magnitude of the bridge angle was correlated solely with the electronic properties of the substituent groups on the phenolic rings. Whereas the strongly electron-donating *tert*-butyl and methyl groups favored the formation of a linear bridge, the electron-withdrawing chloro group influenced the bending of the Fe^{III}–O–Fe^{III} core.[29q]

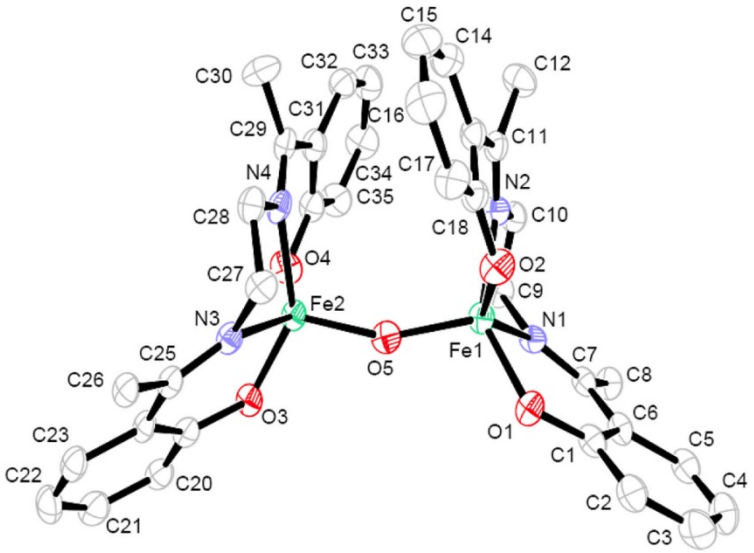

(a)

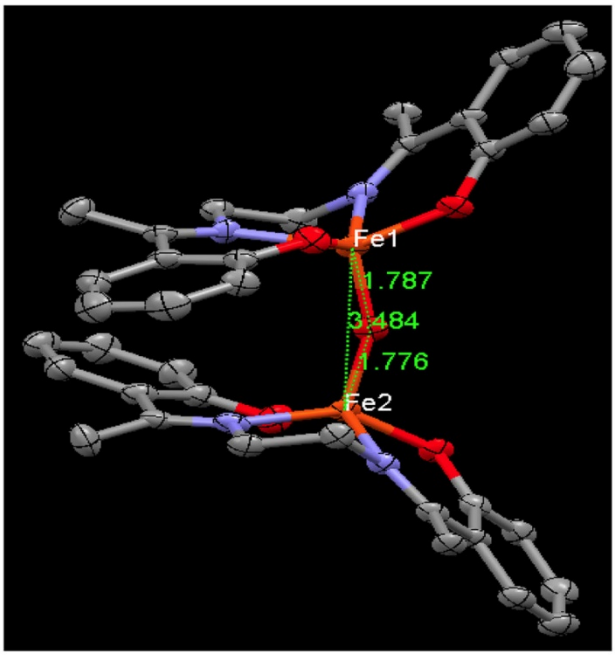

(b)

Figure 5. X-ray structure of [{Fe(hapen)}$_2$(μ-O)].

Each of the two Fe^{III} centers is five-coordinate with four donor atoms provided by the doubly deprotonated (hapen^{2-}) ligand and the fifth donor atom being the μ-oxo atom. The hapen^{2-} donor atoms are two phenolate oxygens and two imine nitrogens. Although the coordination spheres are similar they are not identical as revealed by the values of the angular geometric parameter $\tau = [(\beta-\alpha)/60]$:[30] for Fe(1), $\tau = 0.075$, and for Fe(2), $\tau = 0.116$.

Hence the geometry at the two metal centers is best described as distorted square pyramidal.[29m,n,q] The distorted basal plane is defined by the four donor atoms of hapen^{2-} with the μ-O atom occupying the apical position. As is often the case with such a coordination sphere, the central metal atom is displaced out of the mean basal plane toward the bridging oxygen atom.[32] Since other salen-based μ-oxo-monobridged diiron(III) complexes exhibit the same coordination sphere, it can be assumed that the distorted square-pyramidal geometry is imposed by the nature of the tetradentate Schiff base. The relatively more flexible tripodal ligands have been shown to favor trigonal-bipyramidal structures.[31]

Magnetic Susceptibility Measurements and Mössbauer Spectroscopy

The values of $\chi_M T$ for $[Fe(apMen)_2](ClO_4)_2$ obtained from SQUID measurements varied steadily between 0.008 and 0.090 $cm^3\ K\ mol^{-1}$ over the temperature range 5−300 K, confirming the crystallographic observation that this iron(II) compound exists in the LS state. Magnetic measurements of the other iron(II) compounds $[Fe(apMen)_2]X_2$ (X^- = BPh_4^-, PF_6^-) and $[Fe(apHen)_2]X_2$ (X^- = ClO_4^-, BPh_4^-, PF_6^-) with a Gouy balance at room temperature gave an effective magnetic moment below 0.90 μ_B ($^1A_1$ ground state). The Mössbauer spectrum of $[Fe(apMen)_2](ClO_4)_2$ recorded at 78 K (Supporting Information figure S4) exhibits an LS doublet (ΔE_Q = 1.00 mm s^{-1}, δ = 0.29 mm s^{-1}), corroborating the magnetic data of this compound.

Whereas the pyridyl ketimine apMen stabilizes the LS state of iron(II) the corresponding phenolic ketimine HhapMen favors iron(III) and promotes the $^6A_1 \leftrightarrow {}^2T_2$ ground-state transformation. The magnetic data of three iron(III)-phenolate compounds are presented in figure 6. The plot of the variation of the effective magnetic moment of $[Fe(hapMen)_2]ClO_4$ as a function of absolute temperature (graph B) reveals a very nearly complete stepwise $S = 5/2 \leftrightarrow S = 1/2$ crossover (μ_{eff} = 5.50 μ_B at 400 K and 1.74 μ_B at 5 K). The magnetic moment drops sigmoidally from 400 to 250 K, followed by a steady decrease to 215 K and then a sharper drop to 195 K. The spin transition curve begins to level off at 190 K where the LS state has been fully accessed (μ_{eff} = 1.99 μ_B). $T_{1/2}$ is approximately 330 K and the HS/LS proportion at RT is about 35: 65% (i.e., predominantly LS). Iron(III)-based stepwise spin transitions are rare; to the best of our knowledge none of the closely related X-salRen[15] or (X-sal)$_2$trien[16] iron spin-crossover materials exhibited a two-step spin transition, making [Fe- (hapMen)$_2$]ClO_4 unique in this family of ferric spin-crossover complexes. The influence of counterions on the ferric spin transition in this system is illustrated by the magnetic property of $[Fe(hapMen)_2]BPh_4$ (fig. 6, graph A), whereby replacement of perchlorate by tetraphenylborate stabilizes the HS state (μ_{eff} = 5.61−5.88 μ_B) over the temperature range 5−400 K. On the other hand, the effect of ligand substituents is exemplified by $[Fe(hapEen)_2]ClO_4$, whose spin transition curve (fig. 6, graph C) differs markedly from that of $[Fe(hapMen)_2]ClO_4$ as a consequence of the seemingly trivial replacement of the secondary amine methyl group by an ethyl group. The spin transition in $[Fe(hapEen)_2]ClO_4$ is one-step and follows an incomplete sigmoidal curve. At 400 K, this compound is predominantly high spin (μ_{eff} = 5.08 μ_B), but at room temperature γ_{LS} is just over 80%; $T_{1/2} \approx$ 355 K. Below 165 K, $[Fe(hapEen)_2]ClO_4$ is purely LS (μ_{eff} = 1.99−1.77 μ_B).

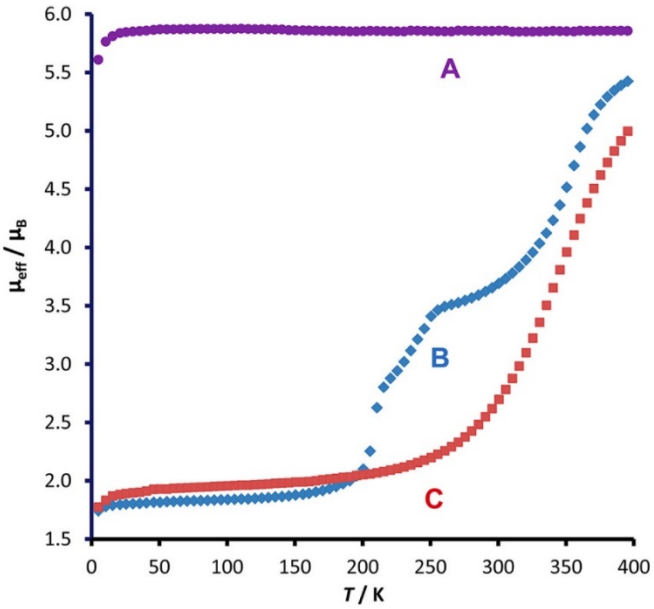

Figure 6. Plots of effective magnetic moment vs absolute temperature for $[Fe(hapMen)_2]BPh_4$ (A), $[Fe(hapMen)_2]ClO_4$ (B), and $[Fe(hapEen)_2]ClO_4$ (C).

The Mössbauer spectra of $[Fe(hapMen)_2]ClO_4$ (fig. 7) are in accord with the magnetic behavior of this SCO compound. At 20 K (where μ_{eff} = 1.80 μ_B), the spectrum exhibits an asymmetric LS doublet (ΔE_Q = 2.74 mm s^{-1}, δ = 0.16 mm s^{-1}). NB: the X-ray structure of this compound at 100 K is also consistent with the $^2T_2$ ground state. At room temperature, the Mössbauer spectrum consists of an outer asymmetric LS doublet (ΔE_Q = 2.47 mm s^{-1}, δ = 0.08 mm s^{-1}) and an inner HS doublet (ΔE_Q = 0.33 mm s^{-1}, δ = 0.10 mm s^{-1}); HS/LS proportions ~30: 70% according to the ratio of the peak areas, which is comparable to the spin composition predicted from magnetic measurements at this temperature.

The magnetic data of the dinuclear iron(III) complex $[\{Fe(hapen)\}_2(\mu\text{-O})]$ were recorded over the temperature range 2−290 K. A graph of μ_{eff} versus T has been plotted in figure 8 to determine parameters for spin−spin coupling. The appearance of this magnetic curve resembles graphs of magnetic data for similar μ-oxo-monobridged diiron(III) complexes exhibiting antiferromagnetic coupling of spins at the metal centers.[29d,f–i,o,p] At room temperature the value of μ_{eff} for $[\{Fe(hapen)\}_2(\mu\text{-O})]$ is 2.63 μ_B, which is considerably smaller than the expected spin-only value of 8.37 μ_B for two uncoupled high-spin iron(III) centers. As can be seen from Figure 8, the magnetic moment decreases with temperature down to 0.38 μ_B around 40 K where the curve levels off to form a plateau probably due to the presence of a paramagnetic monomeric impurity (~0.3%).[29b,d,g–i,o,p]

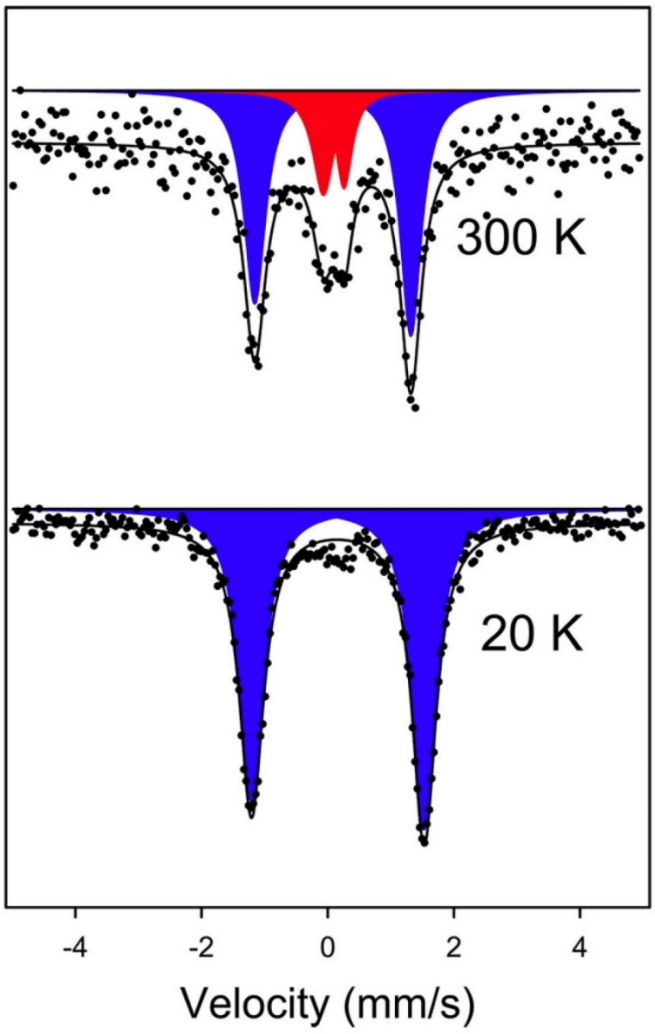

Figure 7. Mössbauer spectra of $[Fe(hapMen)_2]ClO_4$.

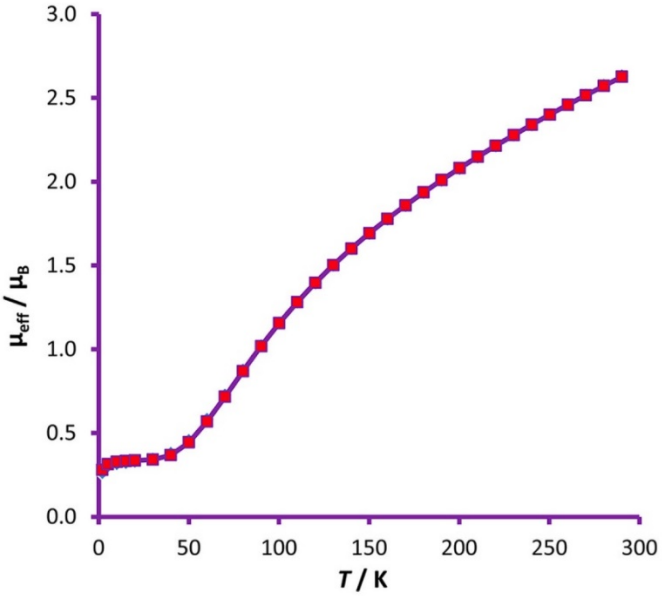

Figure 8. Temperature dependence of the effective magnetic moment of [{Fe(hapen)}$_2$(μ-O)].

Spin−spin coupling in [{Fe(hapen)}$_2$(μ-O)] was determined by the general isotropic spin-exchange Hamiltonian $\hat{H}_{ex} = -2JS_1S_2$[2,29a,b,d,f–i,o,p] ($S1 = S2 = 5/2$). The best fit of the experimental magnetic data gave a J value of −99 cm^{-1} and g = 2.00 with TIP = 1.00 × 10^{-6} cm^3 mol^{-1}.[32] The magnitude and sign of the exchange coupling constant imply strong antiferromagnetic interactions. J values for the vast majority of μ-oxo-monobridged diiron(III) complexes range from ∼−65 to ∼−220 cm^{-1}.[2,29a,b,d,f–i,o,p] Previous studies have correlated the magnitude of the J value with the size of the Fe−O−Fe angle and the Fe−O$_{oxo}$ bond length. The transmission of the spin−spin interactions is believed to be through orbitals on each iron(III) atom and the bridging oxygen atom.[2,29g,i] Therefore, π-bonding across the bridge is often suggested to be the major pathway for antiferromagnetic coupling. In most μ-oxo-monobridged complexes, decreasing the Fe−O−Fe bridge angle from 180° causes a small but significant decrease in the strength of the spin-exchange antiferromagnetic coupling. For example, [{Fe(salen)}$_2$(μ-O)] has an Fe−O−Fe angle of ∼145° with a J value of −92 cm^{-1} [2] and yet the sterically encumbered complex [{Fe(3-^{t}Bu-saltmen)}$_2$O] has an Fe−O−Fe angle of ∼173° with a J value of −100 cm^{-1}.[2] In this work, the J value of −99 cm^{-1} for [{Fe(hapen)}$_2$(μ-O)] is consistent with the Fe−O−Fe angle of ∼155°. Dinuclear iron(III) complexes with a linear (180°) Fe−O−Fe linkage can have J values close to (or above) −200 cm^{-1}.[2,29b,h]

Electron Paramagnetic Spectroscopy

The X-band EPR spectrum of a frozen solution of [Fe(hapMen)$_2$]ClO$_4$ in MeOH at 77 K (Supporting Information figure S5) shows that the low-spin state of this compound at low temperature is retained in solution (g = 2.28, 2.24, 2.19, 1.94).[8a,b] The axial LS signals imply that the unpaired electron of iron(III) resides in a HOMO of d$_{xy}$ character. That [Fe(hapMen)$_2$]ClO$_4$ and [Fe(hapMen)$_2$]ClO$_4$ are isostructural at the metal center is demonstrated by the virtually identical EPR spectra (Supporting Information figure S5). Although in the

solid state $[Fe(hapMen)_2]BPh_4$ is HS (5−400 K), in frozen methanol solution at 77 K, this compound is purely in the doublet ground state.

Electrochemistry

The one-electron reversible oxidative responses for the iron(II)-pyridyl complexes $[Fe(apHen)_2](ClO_4)_2$ and $[Fe(apMen)_2](ClO_4)_2$ at $E_{1/2}° = 0.72$ and 0.82 V (vs SHE), respectively, are attributable to the Fe^{III}/Fe^{II} redox couple. The cyclic voltammogram of $[Fe(apMen)_2](ClO_4)_2$ is displayed in figure 9a. During these redox processes the ligands remained intact. The difference in the redox potentials of these compounds can only be associated with the different amine donor atoms: primary amine for $[Fe(apHen)_2](ClO_4)_2$ and methyl-bearing secondary amine for $[Fe(apMen)_2](ClO_4)_2$. Evidently, the oxidative process of $[Fe(apMen)_2](ClO_4)_2$ is significantly more spontaneous than that of $[Fe(apHen)_2](ClO_4)_2$ ($\Delta G° = -nFE°$). This observation can be explained in terms of the amount of electron density at the metal center of each of these compounds. The methyl group is electron-donating, thus its effect is to stabilize the ferric state and facilitate the oxidation of the ferrous state during the electrochemical process; by so doing the redox potential becomes more positive.[33]

The cyclic voltammogram of the iron(III)−phenolate complex $[Fe(hapMen)_2]ClO_4$ [fig. 9b] shows two electron-transfer processes in the potential range of −1.1 to 2.0 V (vs SHE). The metal-based reversible reductive wave at $E°1/2 = -0.56$ V (vs SHE) is associated with the Fe^{III}/Fe^{II} redox couple. At a higher potential ($E_a = 1.23$ V), a phenoxyl species is generated. Electrochemical oxidations of phenolates and naphtholates to the corresponding phenoxyl and naphthoxyl radicals, respectively, are quite common and are well documented.[34] The electrochemical behavior of the ethyl-substituted complex $[Fe(hapEen)_2]ClO_4$ is identical to that of $[Fe(hapMen)_2]ClO_4$, given the indistinguishable cyclic voltammograms. This result is consistent with the closely matching Hammett parameters[35] of the methyl and ethyl substituents ($\sigma_p = -0.17$ and −0.15, respectively).

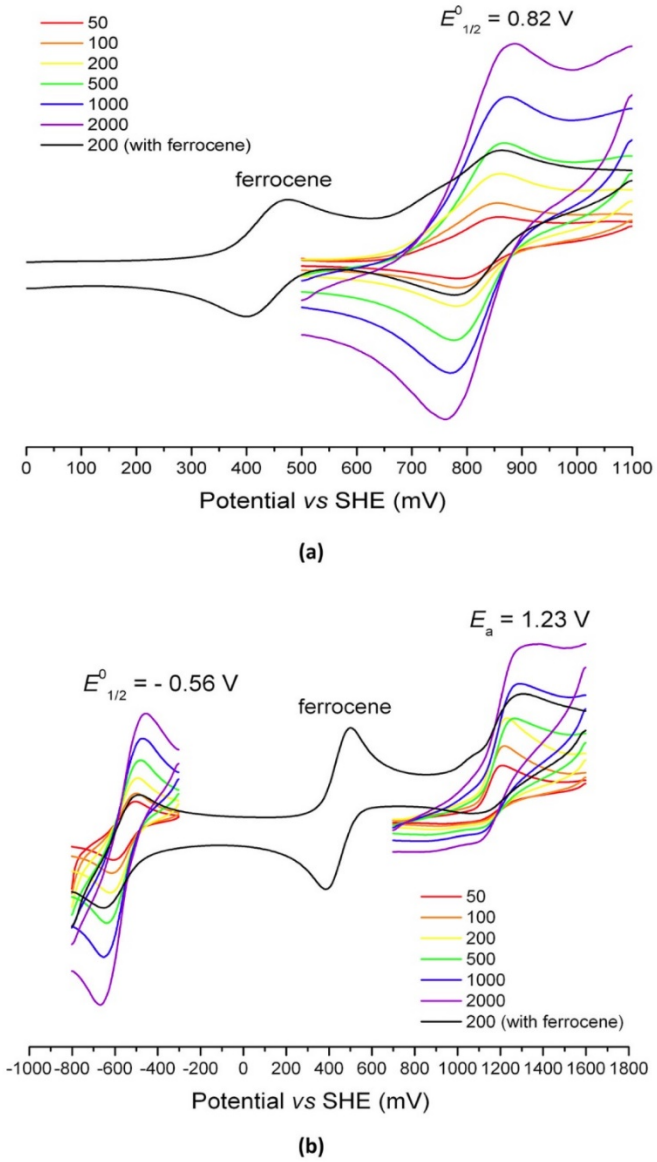

Figure 9. Cyclic voltammograms for (a) $[Fe(apMen)_2](ClO_4)_2$ and (b) $[Fe(hapMen)_2]ClO_4$ in MeCN (clockwise scans).

Electronic Absorption Spectroscopy

The iron(II)− pyridyl compounds $[Fe(apHen)_2]X_2$ ($X^- = ClO_4^-$, BPh_4^-, or PF_6^-) and $[Fe(apMen)_2]X_2$ ($X = ClO_4^-$, BPh_4^-, or PF_6^-) are characterized by intense navy blue and purple-tinged royal blue solutions, respectively, in methanol whereas the iron(III)−phenolate compounds $[Fe(hapMen)_2]X$ ($X^- = ClO_4^-$ or BPh_4^-) and $[Fe(hapEen)_2]ClO_4$ are deep purple-pink in the same solvent. These intense colors originate from the strong visible absorptions (fig. 10a). For each complex cation, the counterion has no effect on the color of the iron compound.

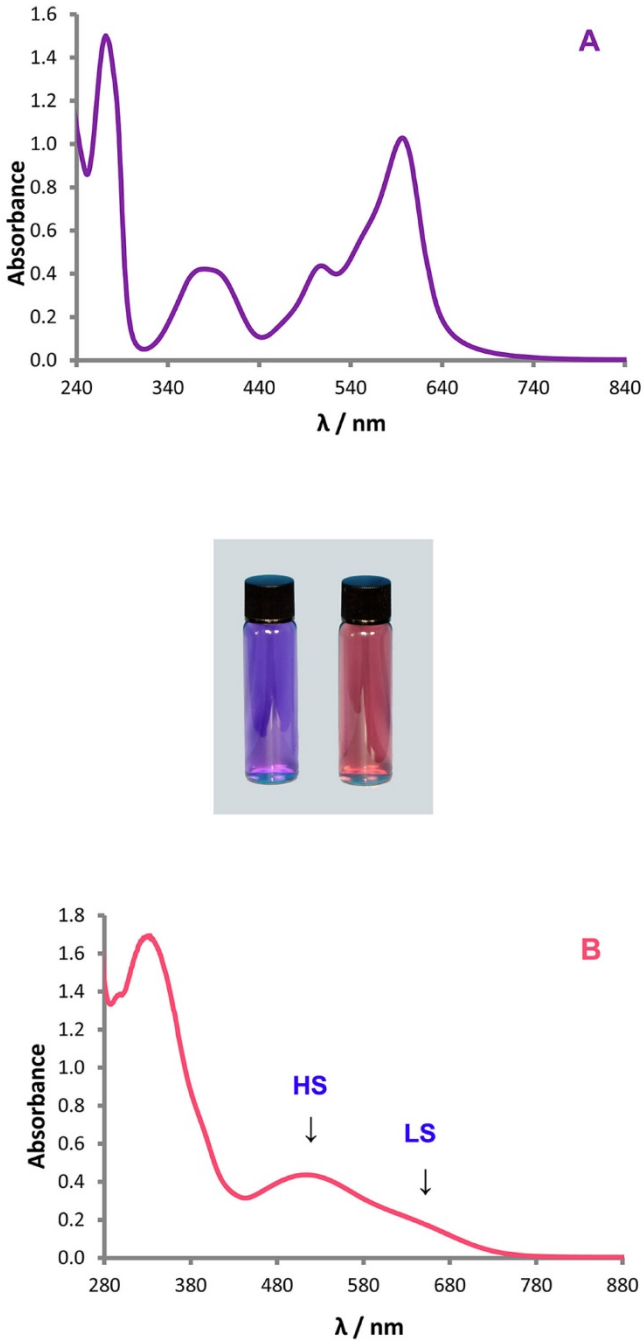

Figure 10. Electronic absorption spectra of $[Fe(apMen)_2](ClO_4)_2$ (A; 0.125 mM, 1-cm path length) and $[Fe(hapMen)_2]ClO_4$ (B; 0.188 mM, 1-cm path length) in MeOH.

The UV−visible spectra of the iron(II) compounds $[Fe(apHen)_2](ClO_4)_2$ and $[Fe(apMen)_2](ClO_4)_2$ resemble each other in accord with the closeness of their colors (navy blue for the former and purplish royal blue for the latter). The strong lobsided absorption bands between 440 and 640 nm [506 nm ($\varepsilon \approx 3500$ M^{-1} cm^{-1}) and 595 nm ($\varepsilon \approx 8200$ M^{-1} cm^{-1})], responsible for the colors, are attributable to charge-transfer transitions in these low-spin

iron(II) compounds. These MLCT transitions represent transference of charge from filled iron(II) d_π orbitals to vacant low-lying p_π^* ligand orbitals. According to the Tanabe−Sugano diagram for octahedral d^6 complexes, several LS spin-allowed ligand-field transitions are possible, but only $^1A_{1g} \rightarrow {}^1T_{1g}$ and $^1A_{1g} \rightarrow {}^1T_{2g}$ occur at relatively low energies.[6b] However, as is often the case with pyridyl-containing LS iron(II) complexes, these d−d transitions were not observed for $[Fe(apHen)_2](ClO_4)_2$ and $[Fe(apMen)_2](ClO_4)_2$ presumably because they were obscured by the hugely intense MLCT absorptions.[36] At higher energies [272 nm ($\varepsilon \approx 12\,000$ M^{-1} cm^{-1}) and 373 nm ($\varepsilon \approx 3350$ M^{-1} cm^{-1})], there are strong absorptions associated with ligand $\pi \rightarrow \pi^*$ transitions. The electronic absorption spectra of the iron(II) compounds presented in this work bear a close resemblance to those of related pyridyl-containing iron(II) complexes.[8a,12,37]

The electronic absorption spectra of the iron(II)−pyridyl ketimines and the corresponding iron(III)−phenolate ketimines contrast as starkly as do the colors of these two classes of iron compounds. The visible spectrum of $[Fe(hapMen)_2]ClO_4$ [fig. 10b] displays two LMCT absorptions,[8b,25,27,33,38] a band at 515 nm ($\varepsilon_{max} = 2330$ M^{-1} cm^{-1}) and a shoulder at 630 nm ($\varepsilon_{max} \approx 1150$ M^{-1} cm^{-1}) ascribable to charge transfer from a phenolate p_π orbital to an iron(III) d_π orbital in the HS and LS states,[15b] respectively. The intense UV absorption ($\lambda_{max} = 330$ nm, $\varepsilon_{max} = 9010$ M^{-1} cm^{-1}) corresponds to the $p_\pi \rightarrow d_\sigma^*$ CT transition. Given that $\Delta_o > P$ for LS Fe(III) and $\Delta_o < P$ for HS Fe(III), there is greater stabilization of the d_π orbitals in LS Fe(III) compounds. Hence the energy separation between the phenolate p_π and iron(III) d_π orbitals in any given octahedral iron(III)−phenolate compound is smaller for the LS state than for the HS state. For this reason, the LS LMCT absorption occurs at longer wavelength than that for the HS state. The same observation was made for $[Fe(hapEen)_2]ClO_4$. The relative intensities of the two LMCT bands indicate the position of the $S = 5/2 \leftrightarrow S = 1/2$ spin equilibrium at 298 K. A similar study has been undertaken previously on the iron(III) salicylaldimine complexes $[Fe(X\text{-salmeen})_2]PF_6$ by Wilson et al.15b In the case of $[Fe(hapMen)_2]BPh_4$, the pure crystalline solid is HS down to 4 K, but undergoes spin conversion in MeOH solution at room temperature; in frozen MeOH solution at 77 K, the transition $^6A_1 \rightarrow {}^2T_2$ is complete as revealed by EPR spectroscopy.

Conclusion

The iron compounds $[Fe(apRen)_2]X_2$ and $[Fe(hapRen)_2]X$ have been generated by reaction of the appropriate tridentate Schiff base (apRen or HhapRen, respectively) with a ferrous or ferric salt in stoichiometric amounts. Illustrative X-ray analyses of $[Fe(apHen)_2](ClO_4)_2$, $[Fe(apMen)_2](ClO_4)_2$, and $[Fe(HapMen)_2]ClO_4$ have provided conclusive evidence for the existence of these iron compounds. The physicochemical properties of $[Fe(apRen)_2X_2$ and $[Fe(hapRen)_2]X$ have been compared and contrasted, and the differences between the pyridyl and phenolate moieties highlighted. Whereas in the former, the ferrous LS ($^1A_1$) state is preferentially stabilized by the pyridyl ketimine irrespective of the type of counterion, in the latter both ferric HS ($^6A_1$) and LS ($^2T_2$) states are supported by the corresponding phenolic ketimine albeit to different extents depending on the type of counterion. In the case of $[Fe(hapMen)_2]ClO_4$ and $[Fe(hapEen)_2]ClO_4$, a seemingly trivial change of amino group, *R*en, triggers a dramatic difference in spin crossover behavior, namely, twostep and one-step $^6A_1 \leftrightarrow {}^2T_2$ transitions, respectively. However, replacement of the counterion ClO_4^- by BPh_4^- renders the resultant iron(III) compound high spin. Interestingly, ESR spectroscopy shows that in frozen MeOH solution, all the iron(III)−phenolate complexes [Fe(hap-

Ren)$_2$]X (X− = ClO_4^- or BPh_4^-) convert quantitatively to the low-spin state. The intense navy and purplish blue colors of $[Fe^{II}(apRen)_2]^{2+}$ derive from strong visible absorptions (440−640 nm) attributable to iron(II) (d_π) → pyridyl (p_π^*) charge-transfer transitions. On the other hand, the deep purple-pink color of $[Fe^{III}(hapRen)_2]^+$ is associated with the phenolate (p_π) → iron(III) (d_π) charge-transfer absorption centered around 515 nm. All the iron(II) and iron(III) compounds are redox-active with reversible metal-centered redox processes. Finally, the dimeric iron(III) complex [{Fe(hapen)}$_2$(μ-O)] exhibits antiferromagnetic coupling of spins mediated by the μ-oxo bridge with a J value of −99 cm^{-1}.

Experimental Section

Materials and Physicochemical Techniques

The pertinent ketones, primary amines, salt precursors, and solvents were commercially available from Sigma-Aldrich at the highest levels of purity possible and used as received. (*Caution:* Perchlorate salts are infamous for explosiveness; hence they must be handled with extreme vigilance in the laboratory. Although problems with such materials were not experienced in the course of this work, only minor explosions occurred during determinations of melting points of the iron compounds possessing perchlorate as counteranion).

Melting points were measured with a Gallenkamp melting point apparatus. Infrared spectra were recorded on a Perkin-Elmer Spectrum BX FT-IR spectrophotometer in the range 4000−400 cm^{-1} using KBr disks of the samples compressed with a Carver hydraulic press. ^{1}H NMR spectra were run on an Avance Bruker 400 DPX spectrometer with DMSO-d_6 as solvent and TMS as internal reference standard. Measurements of UV−visible spectra were carried out on a Hewlett-Packard 8453 diode-array UV−visible spectrophotometer in the range 190−1100 nm using freshly prepared solutions. Microanalyses were performed on a CE440 CHN elemental analyzer. Electron-impact (EI) and fast-atom bombardment (FAB) mass spectra were recorded on a VG 70-SE mass spectrometer with nitrobenzyl alcohol as the matrix.

Variable-temperature magnetic susceptibility measurements were carried out on a Quantum Design MPMS-5S or MPMS-7 SQUID magnetometer operating at a magnetic field of 0.5−1.0 T with HgCo(NCS)4 or palladium as the calibrant. The magnetic data were corrected for diamagnetism the usual way using Pascal's constants. The susceptibility and magnetization of the iron(III) dinuclear complex [{Fe(hapen)}$_2$(μ-O)] were simulated with the program julX for exchange coupled systems designed by E. Bill (Max-Planck-Institut, Mülheim an der Ruhr, Germany).[32] An expression of the Hamilton operator is as follows:

$$\hat{H} = -2J\hat{\vec{S}}_1 \cdot \hat{\vec{S}}_2 + \hat{H}_{ZFS}(\hat{\vec{S}}_1) + \hat{H}_{ZFS}(\hat{\vec{S}}_2)$$

Mössbauer spectra were measured with a conventional constant-acceleration spectrometer equipped with a 50 mCi^{57}Co(Rh) source of γ-rays and a low-temperature accessory. The spectrometer was calibrated with α-Fe at room temperature. X-band EPR spectra were recorded on a Bruker ELEXSYS E-500 CW spectrometer. Cyclic voltammetric experiments were carried out in the range 1100−2000 mV on a model EA9 electrochemical analyzer in distilled MeCN with [Bu$_4$N][PF$_6$] (0.10 M) as the supporting electrolyte using a three-electrode cell made up of a platinum working electrode, a Ag/AgCl reference electrode and a platinum counter electrode. The redox potentials were calibrated with ferrocene as

the internal standard (Fc^+/Fc) and are reported herein relative to the standard hydrogen electrode (SHE) potential.

Syntheses of Schiff Bases and [{Fe(hapen)}$_2$(μ-O)]

The preparative routes to the Schiff-base ligands and the μ-oxo-monobridged iron(III) dimer are described in the Supporting Information.

Synthesis of [Fe(apHen)$_2$](ClO$_4$)$_2$

A colorless mixture of 2-acetylpyridine (0.0969 g, 0.800 mmol) and ethylenediamine (0.0481 g, 0.800 mmol) in MeOH (30 mL) was heated under reflux for 2 h whereupon a light yellow solution was formed. Addition of $Fe(ClO_4)_2 \cdot x\ H_2O$ (0.1019 g, 0.4000 mmol) or $Fe(ClO_4)3 \cdot xH_2O$ (0.1417 g, 0.4000 mmol) yielded a purple-tinged royal blue solution which was heated under reflux for 15 min. The resultant reaction mixture was filtered and kept standing at room temperature for slow evaporation. Black blocks were deposited within three days and isolated by decantation of the mother liquor. Thereafter, this product was washed with ice-cold EtOH and dried in a desiccator over P_4O_{10}. Yield: 0.1125 g (48.39%); m.p.: 228−230°C (explosive). Anal. Calcd for $C_{18}H_{26}N_6Cl_2O_8Fe$: C, 37.20; H, 4.51; N, 14.46. Found: C, 37.11; H, 4.45; N, 14.47. FAB-MS (+ve mode): *m*/*z* = 481, 382, 218. IR data (KBr/cm^{-1}): 3400, 3253, 3208, 3112, 3060, 3042, 2997−2840, 1596, 1589−1453, 1144, 1116, 1090, 627.

Synthesis of [Fe(apHen)$_2$]X$_2$ (X$^-$ = BPh$_4^-$, PF$_6^-$)

The compounds $[Fe(apHen)_2]BPh_4 \cdot H_2O$ and $[Fe(apHen)_2]PF_6$ were synthesized by an analogous procedure to that described above except that the source of the iron(II) ion was $FeCl_2 \cdot 4H_2O$ or FeCl3·6H$_2$O and the counterion NaX (X^- = BPh_4^-, PF_6^-). The appropriate sodium salt, $NaBPh_4$ (0.4107 g, 1.200 mmol) or $NaPF_6$ (0.2015 g, 1.200 mmol), was added to a light yellow solution of $FeCl_2 \cdot 4H_2O$ (0.0795 g, 0.400 mmol) or $FeCl_3 \cdot 6H_2O$ (0.1081 g, 0.4000 mmol) in MeOH (15 mL). The resultant mixture was swirled vigorously and then filtered directly into the hot solution of apHen in MeOH (30 mL), prepared as in the synthesis of $[Fe(apHen)_2](ClO_4)_2$, causing instantaneous color change to purple-tinged royal blue. $[Fe(apHen)_2]PF_6$ was isolated as large black blocks overnight. Yield: 0.1140 g (42.40%). mp: 269−272 °C. Anal. Calcd for $C_{18}H_{26}N_6P_2F_{12}Fe$: C, 32.16; H, 3.90; N, 12.50. Found: C, 32.18; H, 3.88; N, 12.47. FAB-MS (+ve mode): *m*/*z* = 527, 382, 218. IR data (KBr/cm−1): 3337, 3297, 3227, 3193, 3087, 3014, 2975−2857, 1601, 1590−1465, 842, 558. $[Fe(apHen)_2](BPh_4)_2 \cdot 2H_2O$ was obtained as a purple powder immediately after cooling the reaction mixture to room temperature. Yield: 0.2519 g (59.59%). m.p.: 269−273 °C. Anal. Calcd for $C_{66}H_{70}N_6B_2O_2Fe$: C, 75.01; H, 6.68; N, 7.95. Found: C, 75.13; H, 6.57; N, 7.98. FAB-MS (+ve mode): *m*/*z* = 701, 382, 218. IR data (KBr/cm^{-1}): 3400br, 3289, 3244, 3055, 2997−2902, 1597, 1589−1460, 736, 708, 613.

Syntheses of [Fe(apMen)$_2$]X$_2$ (X$^-$ = ClO$_4^-$, BPh$_4^-$, PF$_6^-$)

These iron(II) compounds were produced as described for the corresponding series $[Fe(apMen)_2]X_2$ (X^- = ClO_4^-, BPh_4^-, PF_6^-), but using *N*-methylethylenediamine instead of ethylenediamine. The very pale yellow solution of apMen turned navy blue on treatment with the solution of the appropriate iron(II) or iron(III) salt in MeOH. After brief heating under reflux, the reaction mixture was allowed to stand at room temperature and slowly evaporate. $[Fe(apMen)_2](ClO_4)_2$ crystallized as black blocks within three days. Yield: 0.0955 g (38.1%). m.p.: 212−215°C (explosive). Anal. Calcd for $C_{20}H_{30}N_6Cl_2O_8Fe$: C, 39.43; H, 4.96; N, 15.76.

Found: C, 39.23; H, 4.77; N, 15.61. FAB-MS (+ve mode): *m*/*z* = 509, 410, 232. IR data (KBr/cm^{-1}): 3266, 3169, 3048 3002, 2975−2852, 1598, 1590−1460, 1145, 1119, 1089, 626. [Fe(apMen)$_2$](PF$_6$)$_2$ was obtained as black blocks after a fortnight of solution evaporation. Yield: 0.0563 g (20.1%). m.p.: 188−191°C. Anal. Calcd for $C_{20}H_{30}N_6P_2F_{12}Fe$: C, 34.30; H, 4.32; N, 12.00. Found: C, 34.41; H, 4.38; N, 12.02. FAB MS (+ve mode): *m*/*z* = 555, 410, 232. IR data (KBr/cm−1): 3400br, 3151, 3040, 3010, 2973−2891, 1600, 1589−1463, 842, 559. [Fe(apMen)$_2$](BPh$_4$)$_2$·4H$_2$O was deposited by the solution as a black powder immediately. Yield: 0.1564 g (34.89%). m.p.: 264−267°C. Anal. Calcd for $C_{68}H_{78}N_6B_2O_4Fe$: C, 72.87; H, 7.01; N, 7.50. Found: C, 72.65; H, 6.98; N, 7.52. FAB-MS (+ve mode): *m*/*z* = 729, 410, 232. IR data (KBr/cm^{-1}): 3500br, 3232, 3218, 3160, 3054, 3036, 2997−2891, 1598, 1580−1461, 735, 708, 612.

Syntheses of [Fe(hapMen)$_2$]X (X$^-$ = ClO$_4^-$, BPh$_4^-$)

A yellow mixture of 2′-hydroxyacetophenone (0.1089 g, 0.8000 mmol) and *N*-methylethylenediamine (0.0593 g, 0.800 mmol) in MeOH (30 mL) was heated under reflux for 2 h to afford an intense canary yellow solution. Thereafter, Fe(ClO$_4$)$_3$·*x*H$_2$O (0.1417 g, 0.4000 mmol) or the filtrate of the mixture of FeCl$_3$·6H$_2$O (0.1081 g, 0.4000 mmol) and NaBPh4 (0.4107 g, 1.200 mmol) in MeOH (10 mL) was added, giving an intense purple solution which was heated under reflux for 10 min. Then this reaction mixture was filtered and left standing at room temperature for crystallization. The solution of [Fe(hapMen)$_2$]ClO$_4$ gave black blocks after slow evaporation over a period of five days. Yield: 0.0623 g (27.1%). m.p.: 206−208°C. Anal. Calcd for $C_{22}H_{30}N_4O_6ClFe$: C, 49.13; H, 5.62; N, 10.42. Found: C, 49.15; H, 5.62; N, 10.44. FAB-MS (+ve mode): *m*/*z* = 438, 247, 191. IR data (KBr/cm^{-1}): 3280, 3256, 3008, 2980−2880, 1596, 1580−1435, 1259, 1235, 1120, 1090, 1057, 626. On the other hand, [Fe(hapMen)$_2$]BPh$_4$ crystallized overnight as large irregular-shaped shiny black crystals. Yield: 0.1512 (49.90%). m.p.: 216−217°C. Anal. Calcd for $C_{46}H_{50}N_4O_2BFe$: C, 72.93; H, 6.65; N, 7.40. Found: C, 72.87; H, 6.62; N, 7.43. FAB MS (+ve ion): *m*/*z* = 438, 247, 191. IR data (KBr/cm^{-1}): 3260, 3238, 3055, 3036, 3010, 2981−2873, 1596, 1577−1433, 1267, 1233, 741, 730, 702, 610.

Synthesis of [Fe(hapEen)$_2$]ClO$_4$

This compound was produced as was the analogue [Fe(hapMen)$_2$]ClO$_4$ above save for replacement of *N*-methylethylenediamine by *N*-ethylethylenediamine (0.0705 g, 0.800 mmol). The intense purple solution of [Fe(hapMen)$_2$]ClO$_4$ deposited shiny black needles within two days of slow evaporation. Yield: 0.1013 g (44.74%). m.p.: 232−235°C. Anal. Calcd for $C_{24}H_{34}N_4O_6ClFe$: C, 50.94; H, 6.06; N, 9.90. Found: C, 50.96; H, 6.07; N, 9.91. FAB MS (+ve mode): *m*/*z* = 466, 261, 205. IR data (KBr/cm^{-1}): 3245, 2966−2862, 1595, 1540−1428, 1230, 1120, 1090, 1060, 623.

Single-Crystal X-ray Crystallography

Single-crystal X-ray analyses were performed on Bruker SMART 1K and Bruker SMART APEX-II diffractometers equipped with graphite-monochromated Mo−Kα radiation (λ = 0.71073 Å). The structures were solved by direct methods (SHELXS-97)[39] and refined by full-matrix least-squares based on F_2 (SHELXL-97).[39] Hydrogen atoms were positioned geometrically and allowed to ride on their respective parent atoms. The severely distorted perchlorate counterions of [Fe(apMen)$_2$](ClO$_4$)$_2$ were eliminated by employing the PLATON SQUEEZE function.[21] Details are provided in the relevant CIF.

Associated Content

Supporting Information

Synthetic procedures for ligands and the complex [{Fe(hapen)}$_2$(μ-O)], X-ray crystallographic files of [Fe(apHen)$_2$](ClO$_4$)$_2$, [Fe(apMen)$_2$](ClO$_4$)$_2$, [Fe(hapMen)$_2$]ClO$_4$, H$_2$hapen, and [{Fe(hapen)}$_2$(μ-O)] in CIF format, table of bond distances and angles for [{Fe(hapen)}$_2$(μ-O)], ^{1}H NMR spectrum of H$_2$hapen, EPR spectra of [Fe(hapRen)$_2$]ClO$_4$ (R = Me, Et) in MeOH at 77 K and Mössbauer spectrum of [Fe(apMen)$_2$](ClO$_4$)$_2$. This material is available on the Internet at http://pubs.acs.org.

Acknowledgments – We are greatly indebted to Sultan Qaboos University for financial support (IG/SCI/CHEM/07/02). Research in the Department of Physics and Nebraska Center for Materials and Nanoscience of the University of Nebraska–Lincoln is supported in part by NSF MRSEC Grant DMR-0820521.

References

(1) (a) Sono, M.; Roach, M. P.; Coulter, E. D.; Dawson, J. H. *Chem. Rev.* 1996, *96*, 2841−2887. (b) Lippard, S. J.; Berg, J. M. *Principles of Bioinorganic Chemistry*; University Science Books: Mill Valley, CA, 1994. (c) Bertini, I.; Gray, H. B.; Lippard, S. J.; Valentine, J. S. *Bioinorganic Chemistry*; University Science Books: Sausalito, CA, 1994. (d) Kaim, W.; Schwederski, B. *Bioinorganic Chemistry: Inorganic Elements in the Chemistry of Life*; John Wiley & Sons: Chichester, England, 1994.

(2) Kurtz, D. M., Jr. *Chem. Rev.* 1990, *90*, 585−606.

(3) Cambi, L.; Cagnasso, A. *Atti. Accad. Naz. Lincei, Cl. Sci. Fis. Mat. Nat., Rend.* 1931, *13*, 809−813.

(4) (a) Sim, P. G; Sinn, E. *J. Am. Chem. Soc.* 1981, *103*, 241−243. (b) Morgan, G. G.; Murnaghan, K. D.; Müller-Bunz, H.; McKee, V.; Harding, C. J. Angew. *Chem., Int. Ed.* 2006, *45*, 7192−7195. (c) Liu, Z.; Liang, S.; Di, X.; Zhang, *J. Inorg. Chem. Commun.* 2008, *11*, 783−786. (d) Wang, S.; Ferbinteanu, M.; Marinescu, C.; Dobrinescu, A.; Ling, Q.-D.; Huang, W. *Inorg. Chem.* 2010, *49*, 9839−9851. (e) Gandolfi, C.; Cotting, T.; Martinho, P. N.; Sereda, O.; Neels, A.; Morgan, G. G.; Albrecht, M. *Dalton Trans.* 2011, *40*, 1855−1865.

(5) (a) Faus, J.; Julve, M.; Lloret, F.; Real, J. A.; Sletten, *J. Inorg. Chem.* 1994, *33*, 5535−5540. (b) Sieber, R.; Decurtins, S.; Stoeckli- Evans, H.; Wilson, C.; Yufit, D.; Howard, J. A. K.; Capelli, S. C.; Hauser, A. *Chem.—Eur. J.* 2000, *6*, 361−368. (c) Krivokapic, I.; Zerara, M.; Daku, M. L.; Vargas, A.; Enachescu, C.; Ambrus, C.; Tregenna-Piggott, P.; Amstutz, N.; Krausz, E.; Hauser, A. *Coord. Chem. Rev.* 2007, *251*, 364−378. (d) Kilner, C. A.; Halcrow, M. A. *Dalton Trans.* 2010, *39*, 9008−9012. (e) Graf, M.; Wolmershaüser, G.; Kelm, H.; Demeschko, S.; Meyer, F.; Krüger, H.-J. *Angew. Chem., Int. Ed.* 2010, 49, 950−953. (f) Hayami, S; Komatsu, Y.; Shimizu, T.; Kamihata, H.; Lee, Y. H. *Coord. Chem. Rev.* 2011, 255, 1981−1990. (g) Hayami, S.; Kato, K.; Komatsu, Y.; Fuyuhiro, A.; Ohba, M. *Dalton Trans.* 2011, *40*, 2167−2169.

(6) Examples: (a) Kahn, O.; Martinez, C. *Science* 1998, *279*, 44−48. (b) Gütlich, P.; Garcia, Y.; Goodwin, H. A. *Chem. Soc. Rev.* 2000, *29*, 419−427. (c) Real, J. A.; Gaspar, A. B.; Niel, V.; Muñoz, M. C. *Coord. Chem. Rev.* 2003, *236*, 121−141. (d) Gütlich, P.; Goodwin, H. A. Top. *Curr. Chem.* 2004, *233*, 1−47. (e) Halcrow, M. A. *Polyhedron* 2007, *26*, 3523−3576. (f) Gamez, P.; Costa, J. S.; Quesada, M.; Aromí, G. *Dalton Trans.* 2009, 7845−7853. (g) Halcrow, M. *Coord. Chem. Rev.* 2009, *253*, 2493−2514. (h) Olguin, J.; Brooker, S. *Coord. Chem. Rev.* 2011, 255, 203−240. (j) González-Prieto, R; Fleury, B.; Schramm, F.; Zoppellaro, G.; Chandrasekar, R.; Fuhr, O.; Lebedkin, S.; Kappes, M.; Ruben, M. *Dalton Trans.* 2011, *40*, 7564−7570. (k) Real, J. A.; Andrés, E.; Muñoz, M. C.; Julve, M.; Granier, T.; Bousseksou, A.; Varret, F. *Science* 1995, *268*, 265−267. (l) Mishra, V.; Mishra, H; Mukherjee, R.; Codjovi, E.; Linarès, J.; Létard, J.-F.; Desplanches, C.; Baldé, C.; Enachescu, C.; Varret, F. *Dalton*

Trans. 2009, 7462−7472. (m) Seredyuk, M.; Gaspar, A. B.; Kusz, J.; Bednarek, G.; Gütlich, P. *J. Appl. Crystallogr.* 2007, *40*, 1135−1145.

(7) (a) Gamez, P.; Costa, J. S.; Quesada, M.; Aromí, G. *Dalton Trans.* 2009, 7845−7853. (b) Halcrow, M. A. *Chem. Soc. Rev.* 2011, 40, 4119−4142. (c) Tao, J.; Wei, R.-J.; Huang, R.-B.; Zheng, L.-S. Chem. *Soc. Rev.* 2012, *41*, 703−737.

(8) Examples: (a) Shongwe, M. S.; Al-Rahbi, S. H.; Al-Azani, M. A.; Al-Muharbi, A. A.; Al-Mjeni, F.; Matoga, D.; Gismelseed, A.; Al-Omari, I. A.; Yousif, A.; Adams, H.; Morris, M. J.; Mikuriya, M. *Dalton Trans.* 2012, *41*, 2500−2514. (b) Shongwe, M. S.; Al-Rashdi, B. A.; Adams, H.; Morris, M. J.; Mikuriya, M.; Hearne, G. R. *Inorg. Chem.* 2007, *46*, 9558−9568. (c) Hearne, G. R.; Munro, O.; Pearson, N.; Shongwe, M. *J. Phys.: Condens. Matter* 2005, *17*, S727−S742. (d) Nihei, M.; Shiga, T.; Maeda, Y.; Oshio, H. *Coord. Chem. Rev.* 2007, *251*, 2606−2621. (e) Hayami, S.; Hiki, K.; Kawahara, T.; Maeda, Y.; Urakami, D.; Inoue, K.; Ohama, M.; Kawata, S.; Sato, O. *Chem.—Eur. J.* 2009, *15*, 3497−3508. (f) Ross, T. M.; Neville, S. M.; Innes, D. S.; Turner, D. R.; Moubaraki, B.; Murray, K. S. *Dalton Trans.* 2010, *39*, 149−159. (g) Ortega-Villa, N. A.; Muñoz, M. C.; Real, J. A. *Eur. J. Inorg. Chem.* 2010, 5563−5567. (h) Griffin, M.; Shakespeare, S.; Shepherd, H. J.; Harding, C. J.; Létard, J.-F.; Desplanches, C.; Goeta, A. E.; Howard, J. A. K.; Powell, A. K.; Mereacre, V.; Garcia, Y.; Naik, A. D.; Müller-Bunz, H.; Morgan, G. G. Angew. *Chem., Int. Ed.* 2011, *50*, 896−900. (i) Tang, J.; Costa, J. S.; Smulders, S.; Molnár, G.; Bousseksou, A.; Teat, S. J.; Li, Y.; van Albada, G. A.; gamez, P.; Reedijk, *J. Inorg. Chem.* 2009, *48*, 2128−2135. (j) Gandolfi, C.; Moitzi, C.; Schurtenberger, P.; Morgan, G. G.; Albrecht, M. *J. Am. Chem. Soc.* 2008, 130, 14434− 14435. (k) Pritchard, R.; Barrett, S. A.; Kilner, C. A.; Halcrow, M. A. *Dalton Trans.* 2008, 3159−3168. (l) Hayami, S.; Gu, Z.; Yoshiki, H.; Fujishima, A.; Sato, O. J. Am. Chem. Soc. 2001, 123, 11644−11650.

(9) (a) Boinnard, D.; Bousseksou, A.; Dworkin, A.; Savariault, J.-M.; Varret, F.; Tuchagues, J.-P. *Inorg. Chem.* 1994, *33*, 271−281. (b) Salmon, L.; Bousseksou, A.; Donnadieu, B.; Tuchagues, J.-P. *Inorg. Chem.* 2005, *44*, 1763−1773. (c) Weber, B; Bauer, W.; Obel, J. Angew. *Chem., Int. Ed.* 2008, *47*, 10098−10101. (d) Weber, B.; Carbonera, C.; Desplances, C.; Létard, J.-F. *Eur. J. Inorg. Chem.* 2008, 1589−1598. (e) Weber, B. Coord. *Chem. Rev.* 2009, 253, 2432−2449. (f) Weber, B.; Bauer, W.; Pfaffeneder, T.; Dîrtu, M. M.; Naik, A. D.; Rotaru, A.; Garcia, Y. *Eur. J. Inorg. Chem.* 2011, 3193−3206. (g) Schlamp, S.; Weber, B.; Naik, A. D.; Garcia, Y. *Chem. Commun.* 2011, *47*, 7152−7154. (h) Zhang, L.; Xu, G.-C.; Xu, H.-B.; Zhang, T.; Wang, Z.-M.; Yuan, M.; Gao, S. *Chem. Commun.* 2010, *46*, 2554−2556. (i) Zhang, Li; Xu, G.-C.; Xu, H.-B.; Mereacre, V.; Wang, Z.-M.; Powell, A. K.; Gao, S. *Dalton Trans.* 2010, 39, 4856−4868.

(10) (a) Sunatsuki, Y.; Sakata, M.; Matsuzaki, S.; Matsumoto, N.; Kojima, M. *Chem. Lett.* 2001, 1354−1355. (b) Sunatsuki, Y.; Ikuta, Y.; Matsumoto, N.; Ohta, H.; Kojima, M.; Hayami, S.; Maeda, Y.; Kaizaki, S.; Dahan, F.; Tuchagues, J.-P. Angew. *Chem., Int. Ed.* 2003, 42, 1614− 1618. (c) Ohta, H.; Sunatsuki, Y.; Kojima, M.; Iijima, S.; Akashi, H.; Matsumoto, *N. Chem. Lett.* 2004, *33*, 350−351. (d) Sunatsuki, Y.; Ohta, H.; Kojima, M.; Ikuta, Y.; Goto, Y.; Matsumoto, N.; Iijima, S.; Akashi, H.; Kaizaki, S.; Dahan, F.; Tuchagues, J.-P. *Inorg. Chem.* 2004, *43*, 4154−4171. (e) Brewer, C.; Brewer, G.; Butcher, R. J.; Carpenter, E. E.; Cuenca, L.; Noll, B. C.; Scheidt, W. R.; Viragh, C.; Zavalij, P. Y.; Zielaski, D. *Dalton Trans.* 2006, 1009−1019.

(11) (a) Zhu, D; Xu, Y.; Yu, Z.; Guo, Z.; Sang, H.; Liu, T.; You, X. *Chem. Mater.* 2002, 14, 838−843. (b) Bréfuel, N.; Duhayon, C.; Shova, S.; Tuchagues, J.-P. *Chem. Commun.* 2007, 5223−5225. (c) Kitchen, J. A.; Jameson, G. N. L.; Tallon, J. L.; Brooker, S. *Chem. Commun.* 2010, 46, 3200−3202. (d) Basegawa, Y.; Takahashi, K.; Kume, S.; Nishihara, H. *Chem. Commun.* 2011, 47, 6846−6848. (e) Bao, X.; Guo, P.-H.; Liu, J.-L.; Leng, J.-D.; Tong, M.-L. *Chem.–Eur. J.* 2011, *17*, 2335− 2339.

(12) Krumolz, P. *Inorg. Chem.* 1965, *4*, 612−616.

(13) Banerjee, S.; Gangopadhyay, J.; Lu, C.-Z.; Chen, J.-T.; Ghosh, A. *Eur. J. Inorg. Chem.* 2004, 2533−2541.

(14) (a) Chattopadhyay, R.; Drew, M. G. B.; Figuerola, A.; Diaz, C.; Ghosh, A. *Polyhedron* 2006, *25*, 2241−2253. (b) Miao, J.-Y. *Synth. React. Inorg. Met.-Org. Nano-Met. Chem.* 2011, *41*, 689−693.

(15) (a) Summerton, A. P.; Diamantis, A. A.; Snow, M. R. *Inorg. Chim. Acta* 1978, *27*, 123−128. (b) Petty, R. H.; Dose, E. V.; Tweedle, M. F.; Wilson, L. J. *Inorg. Chem.* 1978, *17*, 1064−1071. (c) Haddad, M. S.; Federer, W. D.; Lynch, M. W.; Hendrickson, D. N. *J. Am. Chem. Soc.* 1980, *102*, 1468−1470. (d) Haddad, M. S.; Lynch, M. W.; Federer, W. D.; Hendrickson, D. N. *Inorg. Chem.* 1981, *20*, 123−131. (e) Haddad, M. S.; Federer, W. D.; Lynch, M. W.; Hendrickson, D. N. *Inorg. Chem.* 1981, *20*, 131−139. (f) Sim, P. G.; Sinn, E.; Petty, R. H.; Merrill, C. L.; Wilson, L. J. *Inorg. Chem.* 1981, *20*, 1213−1222. (g) Timken, M. D.; Hendrickson, D. N.; Sinn, E. *Inorg. Chem.* 1985, *24*, 3947−3955. (h) Hayami, S.; Miyazaki, S.; Yamamoto, M.; Hiki, K.; Motokawa, N.; Shuto, A.; Inoue, K.; Shinmyozu, T.; Maeda, Y. *Bull. Chem. Soc. Jpn.* 2006, *79*, 442−450. (i) Faulmann, C.; Jacob, K.; Dorbes, S.; Lampert, S.; Malfant, I.; Doublet, M.-L.; Valade, L.; Real, J. A. *Inorg. Chem.* 2007, *46*, 8548−8559.

(16) (a) Tweedle, M. F.; Wilson, L. J. *J. Am. Chem. Soc.* 1976, *98*, 4824−4834. (b) Nishida, Y.; Kino, K.; Kida, S. *J. Chem. Soc., Dalton Trans.* 1987, 1957−1961. (c) Dorbes, S.; Valade, L.; Real, J. A.; Faulmann, C. *Chem. Commun.* 2005, 69−71. (d) Gandolfi, C.; Moitzi, C.; Schurtenberger, P.; Morgan, G. G.; Albrecht, M. J. *Am. Chem. Soc.* 2008, *130*, 14434−14435. (e) Martinho, P. N.; Harding, C. J.; Müller-Bunz, H.; Albrecht, M.; Morgan, G. G. *Eur. J. Inorg. Chem.* 2010, 675− 679.

(17) (a) Gao, W. T.; Zheng, Z. *Molecules* 2002, *7*, 511−516. (b) Boghaei, D. M.; Mohebi, S. *J. Mol. Catal. A: Chem.* 2002, *179*, 41− 51.

(18) Examples: (a) Yamada, M.; Ooidemizu, M.; Ikuta, Y.; Osa, S.; Matsumoto, N.; Iijima, S.; Kojima, M.; Dahan, F.; Tuchagues, J.-P. *Inorg. Chem.* 2003, 42, 8406−8416. (b) Holland, J. M.; McAllister, J. A.; Kilner, C. A.; Thornton-Pett, M.; Bridgeman, A. J.; Halcrow, M. A. *J. Chem. Soc., Dalton Trans.* 2002, 548−554. (c) Kennedy, B. J.; McGrath, A. C.; Murray, K. S.; Skelton, B. W.; White, A. H. *Inorg. Chem.* 1987, *26*, 483−495.

(19) Shongwe, M. S.; Al-Kharousi, H. N. R.; Adams, H.; Morris, M. J.; Bill, E. *Inorg. Chem.* 2006, 45, 1103−1107.

(20) Tanimura, K.; Kitashima, R.; Bréfuel, N.; Nakamura, M.; Matsumoto, N.; Shova, S.; Tuchagues, J.-P. *Bull. Chem. Soc. Jpn.* 2005, 78, 1279−1282.

(21) (a) Spek, A. L. *Acta Crystallogr., Sect. A* 1990, *46*, C40. (b) Spek, A. L. *PLATON, A Multipurpose Crystallographic Tool*; Utrecht University: Utrecht, The Netherlands, 1998. (c) Spek, A. L. *J. Appl. Crystallogr.* 2003, *36*, 7−13.

(22) (a) Hayami, S.; Kawajiri, R.; Juhász, G.; Kawahara, T.; Hashiguchi, K.; Sato, O.; Inoue, K.; Maeda, Y. *Bull. Chem. Soc. Jpn.* 2003, *76*, 1207−1213. (b) Anđelković, K.; Sladić, D.; Bacchi, A.; Pelizzi, G.; Filipović, N.; Rajković, M. *Trans. Metal Chem.* 2005, *30*, 243−250.

(23) Zhang, Li; Xu, G.-C.; Xu, H.-B.; Mereacre, V.; Wang, Z.-M.; Powell, A. K.; Gao, S. *Dalton Trans.* 2010, *39*, 4856−4868.

(24) Examples: (a) Zhang, Li; Xu, G.-C.; Xu, H.-B.; Zhang, T.; Wang, Z.-M.; Y., M.; Gao, S. *Chem. Commun.* 2010, 46, 2554−2556. (b) Bernhardt, P. V.; Chin, P.; Sharpe, P. C.; Richardson, D. R. *Dalton Trans.* 2007, 3232−3244. (c) Tao, J.-Q.; Gu, Z.-G.; Wang, T.-W.; Yang, Q.-F.; Zuo, J.-L.; You, X.-Z. *Inorg. Chim. Acta* 2007, 360, 4125−4132. (d) Diebold, A.; Hagen, K. S. *Inorg. Chem.* 1998, *37*, 215−225.

(25) (a) Shakya, R.; Allard, M. M.; Johann, M.; Heeg, M. J.; Rentschler, E.; Shearer, J. M.; McGarvey, B.; Verani, C. N. *Inorg. Chem.* 2011, *50*, 8356−8366. (b) Imbert, C.; Hratchian, H. P.; Lanznaster, M.; Heeg., M. J.; Hryhorczuk, L. M.; McGarvey, B. R.; Schlegel, H. B.; Verani, C. N. *Inorg. Chem.* 2005, *44*, 7414−7422.

(26) (a) Kannappan, R.; Tanase, S.; Mutikainen, I.; Turpeinen, U.; Reedijk, J. *Polyhedron* 2006, *25*, 1646−1654. (b) Sreerama, S. G.; Mukhopadyay, A.; Pal, S. *Inorg. Chem. Commun.* 2006, *9*, 1083−1086.

(27) (a) Shongwe, M. S.; Kaschula, C. H.; Adsetts, M. S.; Ainscough, E. W.; Brodie, A. M.; Morris, M. *J. Inorg. Chem.* 2005, *44*, 3070−3079. (b) Matoga, D.; Szklarzewicz, J.; Stadnicka, K.; Shongwe, M. S. *Inorg. Chem.* 2006, *46*, 9042−9044.

(28) Corden, J. P.; Errington, W.; Moore, P.; Wallbridge, M. G. H. *Acta Crystallogr.* 1997, *C53*, 486−488.

(29) (a) Min, K. S.; Rhinegold, A. L.; Miller, J. S. *J. Am. Chem. Soc.* 2006, *128*, 40−41. (b) Tanase, S.; Gallego, P. M.; Bouwman, E.; Long, G. J.; Rebbouh, L.; Grandjean, F.; de Gelder, R.; Mutikainen, I.; Turpeinen, U.; Reedijk, J. *Dalton Trans.* 2006, 1675−1684. (c) Li, F.; Wang, M.; Ma, C.; Gao, A.; Chen, H.; Sun, L. *Dalton Trans.* 2006, 2427−2434. (d) Junk, P. C.; McCool, B. J.; Moubaraki, B.; Murray, K. S.; Spiccia, L.; Cashion, J. D.; Steed, J. W. *Dalton Trans.* 2002, 1024−1029. (e) Darensbourg, D. J.; Ortiz, C. G.; Billodeaux, D. R. *Inorg. Chim. Acta* 2004, *357*, 2143−2149. (f) Pardo, E.; Lloret, F.; Carrasco, R.; Muñoz, M. C.; Temporal-Sánchez, T.; Ruiz-García, R. *Inorg. Chim. Acta* 2004, 357, 2713−2720. (g) Min, K. S.; Arif, A. M.; Miller, J. S. *Inorg. Chim. Acta* 2007, *360*, 1854−1858. (h) Majumder, A.; Pilet, G.; El Fallah, M. S.; Ribas, J.; Mitra, S. *Inorg. Chim. Acta* 2007, *360*, 2307−2312. (i) Kreher, U.; Hearn, M. T. W.; Moubaraki, B.; Murray, K. S.; Spiccia, L. *Polyhedron* 2007, *26*, 3205−3216. (j) Cheng, L.; Lee, J.; Powell, D. R.; Richter-Addo, G. B. *Acta Crystallogr.* 2004, *E60*, m1340−m1342. (k) Egdal, R. K.; Hazell, A.; McKenzie, C. J. *Acta Crystallogr.* 2002, *E58*, m10−m12. (l) Duban, E. A.; Drebushchak, T. N.; Bryliakov, K. P.; Talsi, E. P. *Mendeleev Commun.* 2007, *17*, 291−293. (m) Davies, J. E.; Gatehouse, B. M. *Acta Crystallogr.* 1973, *B29*, 1934−1942. (n) Koner, S.; Iijima, S.; Watanabe, M.; Sato, M. J. *Coord. Chem.* 2003, *56*, 103−111. (o) Pilz, M. F.; Limberg, C.; Demeshko, S.; Meyer, F.; Ziemer, B. *Dalton Trans.* 2008, 1917−1923. (p) Li, A.-R.; Wei, H.-H.; Gang, L.-L. *Inorg. Chim. Acta* 1999, *290*, 51−56. (q) Strautmann, J. B. H.; von Richthofen, C.-G. F.; Heinze-Brückner, G.; DeBeer, S.; Bothe, E; Bill, E.; Weyhermüler; Stammler, A.; Böggle, H.; Glaser, T. *Inorg. Chem.* 2011, *50*, 155−171.

(30) Addison, A. W.; Rao, T. N.; Reedijk; van Rijn, J.; Verschoor, G. C. *J. Chem. Soc., Dalton Trans.* 1984, 1349−1356.

(31) (a) Hwang, J. W.; Govindaswamy, K.; Koch, S. A. *Chem. Commun.* 1998, 1667−1668. (b) Hasan, K.; Fowler, C.; Kwong, P.; Crane, A. K.; Collins, J. L.; Kozak, C. M. *Dalton Trans.* 2008, 2991−2998. (c) Safaei, E.; Sheykhi, H.; Weyhermüller, T.; Bill, E. *Inorg. Chim. Acta* 2012, *384*, 69−75.

(32) Bill, E. http://ewww.mpi-muelheim.mpg.de/bac/logins/bill/julX_en.php, 2008.

(33) Lanznaster, M.; Neves, A.; Bortoluzzi, A. J.; Assumpção, A. M. C.; Vencato, I.; Machado, S. P.; Drechsel, S. M. *Inorg. Chem.* 2006, *45*, 1005−1011.

(34) (a) Allard, M. M.; Sonk, J. A.; Heeg, M. J.; McGarvey, B. R.; Schlegel, H. B.; Verani, C. N. *Angew. Chem., Int. Ed.* 2012, *51*, 3178−3182. (b) Richardson, D. R.; Bernhardt, P. V. *J. Biol. Inorg. Chem.* 1999, *4*, 266−273. (c) Bernhardt, P. V.; Chin, P.; Sharpe, P. C.; Richardson, D. R. *Dalton Trans.* 2007, 3232−3244. (d) Stockheim, C.; Hoster, L.; Weyhermüller, T.; Wieghardt, K.; Nuber, B. *Dalton Trans.* 1996, 4409−4416.

(35) Hansch, C.; Leo, A.; Taft, R. W. *Chem. Rev.* 1991, *91*, 165−195.

(36) (a) Atkins, P. W.; Overton, T. L.; Rourke, J. P.; Weller, M. T.; Armstrong, F. A. *Shriver and Atkins' Inorganic Chemistry*, 5th ed.; Oxford University Press: Oxford, U.K., 2010. (b) Cotton, F. A.; Wilkinson, G.; Murillo, C. A.; Bochmann, M. *Advanced Inorganic Chemistry*, 6th ed.; John Wiley & Sons: New York, 1999.

(37) (a) Baggio-Saitovitch, E.; de Paoli, M. A. *Inorg. Chim. Acta* 1978, 27, 15−20. (b) Ramesh, K.; Mukherjee, R. N. *Indian J. Chem.* 1991, *30A*, 1057−1059. (c) Huang, W.; Ogawa, T. *J. Mol. Struct.* 2006, *785*, 21−26.

(38) (a) Shongwe, M. S.; Smith, C. A.; Ainscough, E. W.; Baker, H. M.; Brodie, A. M.; Baker, E. N. *Biochemistry* 1992, *31*, 4451−4458. (b) Shongwe, M. S.; Smith, R.; Marques, H. M.; van Wyk, J. A. *J. Inorg. Biochem.* 2004, 98, 199−208. (c) Gaber, B. P.; Miskowski, V.; Spiro, T. G. *J. Am. Chem. Soc.* 1974, *96*, 6868−6873.

(39) Sheldrick, G. M. *Acta Crystallogr.* 2008, *A64*, 112−122.

Supplementary Information

Syntheses of Schiff bases and [{Fe(hapen)}2(μ-O)]

Syntheses of Tridentate Schiff Bases

Each of the phenolic ligands HhapRen (R = Me, Et) and pyridyl ligands apRen (R = H, Me) was generated *in situ* by condensation reaction of the appropriate combination of ketone and primary amine, and subsequently complexed directly with iron(III) or iron(II), respectively. They were isolated as viscous liquids for spectroscopic measurements. The synthesis of HhapMen illustrates the preparative route to these Schiff bases. To a colorless solution of 2′-hydroxyacetophenone (0.1089 g, 96.30 μL, 0.80 mmol) in absolute EtOH (30 mL) was added *N*-methylethylenediamine (0.0593 g, 70.51 μL, 0.80 mmol) with instantaneous formation of a pale yellow mixture. Upon heating under reflux, the colour of the solution developed progressively with time to canary yellow. After two hours of refluxing, the reaction mixture was stripped of the solvent on the rotor evaporator to afford a dark orange syrupy liquid of HhapMen. The other Schiff bases were synthesised following an identical procedure; however, whereas the phenolic ligands gave canary solutions, the pyridyl Schiff bases formed weakly colored solutions gradually: light yellow for apHen and very pale yellow for apMen. Selected spectral data for **HhapMen**: ^{1}H NMR data (DMSO-d_6): δ 16.38 (br, s), 7.36 (d, J = 7.8 Hz), 7.01 (t, J = 7.6 Hz), 6.51 (d, J = 8.3 Hz), 6.47 (t, J = 7.6 Hz), 3.38 (t, J = 6.3 Hz), 2.55 (t, J = 6.4 Hz), 2.11 (s), 2.09 (s). UV-vis (DMSO, λ_{max}/nm): 320, 395. Selected spectral data for **HhapEen**: ^{1}H NMR data (DMSO-d_6): δ 16.40 (br, s), 7.41 (d, J = 7.8 Hz), 7.06 (t, J = 7.6 Hz), 6.56 (d, J = 8.1 Hz), 6.52 (t, J = 7.5 Hz), 3.42 (t, J = 6.4 Hz), 2.64 (t, J = 6.5 Hz), 2.39 (q, 7.0 Hz), 2.16 (s), 0.83 (t, J = 7.1 Hz). UV-vis (DMSO, λ_{max}/nm): 320, 395. Selected spectral data for **apHen**: UV-vis (DMSO, λ_{max}/nm): 385br,sh. Selected spectral data for **apMen**: UV-vis (DMSO, λ_{max}/nm): 370br,sh.

Synthesis of H2hapen

Ethylenediamine (0.1503 g, 167.1 μL, 2.500 mmol) was dissolved in EtOH (50 mL) to give a colorless solution which upon addition of 2′-hydroxyacetophenone (0.6808 g, 601.9 μL, 5.000 mmol) turned greenish yellow immediately. The resultant reaction mixture was heated under reflux for 2 hours, during which time the color turned fluorescent yellow and the product started to crystallize. However, the process of crystallization was allowed to continue overnight at room temperature. Subsequently, the product was filtered off by suction on the Buchner funnel and washed with ice-cold EtOH. Finally, the bright yellow needles were dried in a desiccator over P_4O_{10}. Yield: 0.5617 g (75.81%); m.p.: 197−199°C. Anal. Calcd for $C_{18}H_{20}N_2O_2$: C, 72.95; H, 6.80; N, 9.45. Found: C, 72.99; H, 6.77; N, 9.47. EI-MS: m/z = 296, 161. IR data (KBr/cm^{-1}): 3450br, 3055, 2940–2830, 1611, 1580–1445, 1292, 1239. ^{1}H NMR data ($CDCl_3$): δ 15.90 (br, s), 7.52 (dd, J = 8.0, 1.6 Hz), 7.29 (ddd, J = 8.3, 7.4, 1.6 Hz), 6.91 (dd, J = 8.3, 1.1 Hz), 6.79 (ddd, J = 8.0, 7.4, 1.1 Hz), 3.97 (s), 2.38 (s). UV-vis [DMSO, λ_{max}/nm (ε/L mol^{-1} cm^{-1})]: 320 (8070), 400 (1600).

Synthesis of [{Fe(hapen)}2(μ-O)]

This dimeric complex was synthesised either directly from the ligand produced *in situ* or the isolated ligand in a stepwise process.

Method I. 2′-Hydroxyacetophenone (0.1089 g, 0.800 mmol) and excess ethylenediamine (0.0481 g, 0.800 mmol) were combined in MeOH (30 mL) to afford a light greenish yellow solution which was heated under reflux for 1 hour during which time the color of the mixture turned fluorescent greenish yellow. Then to this mixture was added $Fe(ClO_4)_3{\cdot}xH_2O$ (0.1417 g, 0.4000 mmol) or $Fe(ClO_4)_2{\cdot}xH_2O$ (0.1019 g, 0.4000 mmol), yielding a red-brown solution which was heated under reflux for 10 minutes. Thereafter, the mixture was filtered and kept at room temperature for crystallization. Within two days, shiny red blocks appeared and were isolated by decantation, followed by washing with ice-cold EtOH. This product was dried in air and later in the desiccator over P_4O_{10}. Yield: 0.0633 g (22.1%); m.p.: 321–322°C.

Method II. To a yellow suspension of H2hapen (0.1185 g, 0.4000 mmol) in MeOH (30 mL) was added $Fe(ClO_4)_3{\cdot}xH_2O$ (0.1417 g, 0.4000 mmol) or $Fe(ClO_4)_2{\cdot}xH_2O$ (0.1019 g, 0.4000 mmol) whereupon a dark red-brown solution was formed. This reaction mixture was heated under reflux for 15 minutes and then filtered. On standing at room temperature, the solution afforded shiny red blocks within two days. The crystals were isolated by decantation, washed with ice-cold EtOH and then dried in a desiccator over P_4O_{10}. Yield: 0.0675 g (23.6%); m.p.: 321–322°C. Anal. Calcd for $C_{36}H_{36}N_4O_5Fe_2$: C, 60.36; H, 5.06; N, 7.82. Found: C, 60.33; H, 5.02; N, 7.80. FAB-MS (+ve ion): *m*/*z* = 716, 700, 366, 350, 307, 216, 190. IR data (KBr/cm^{-1}): 3090, 3055, 3011, 2989–2835, 1598, 1572(sh)–1437, 1236, 843, 422.

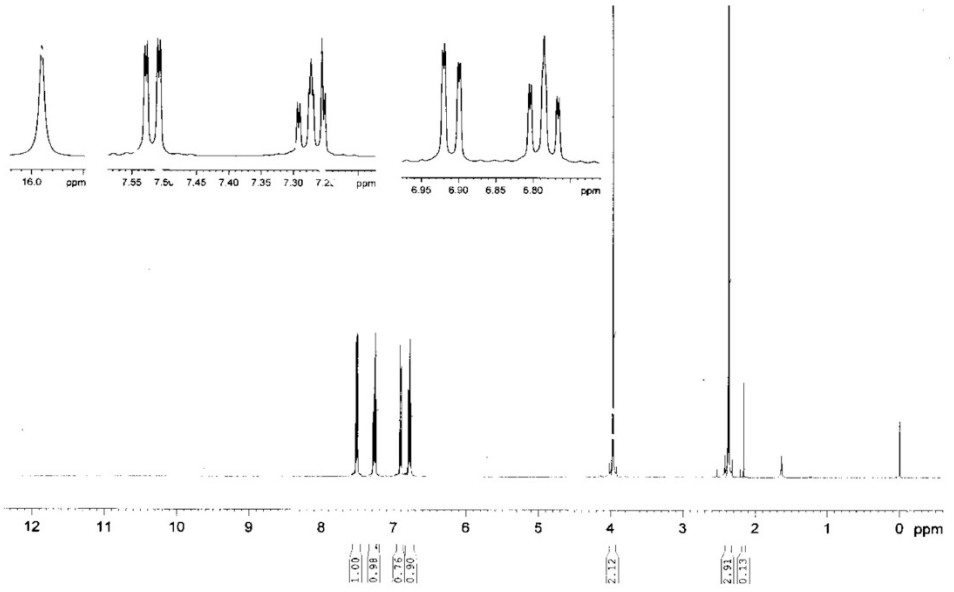

Figure S1. ^{1}H NMR spectrum of H2hapen in $CDCl_3$.

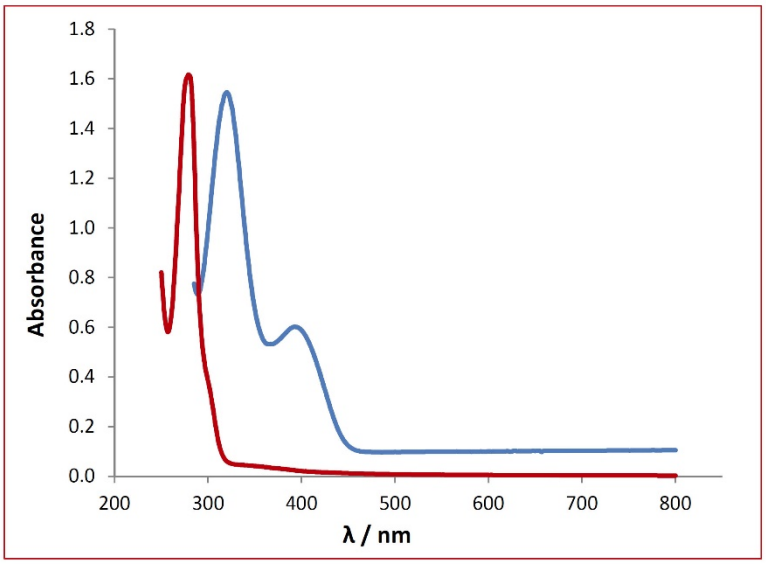

Figure S2. Electronic absorption spectra of the Schiff base HhapMen (blue) and its reduced form (red) in DMSO (0.40 mM, 1-cm path length).

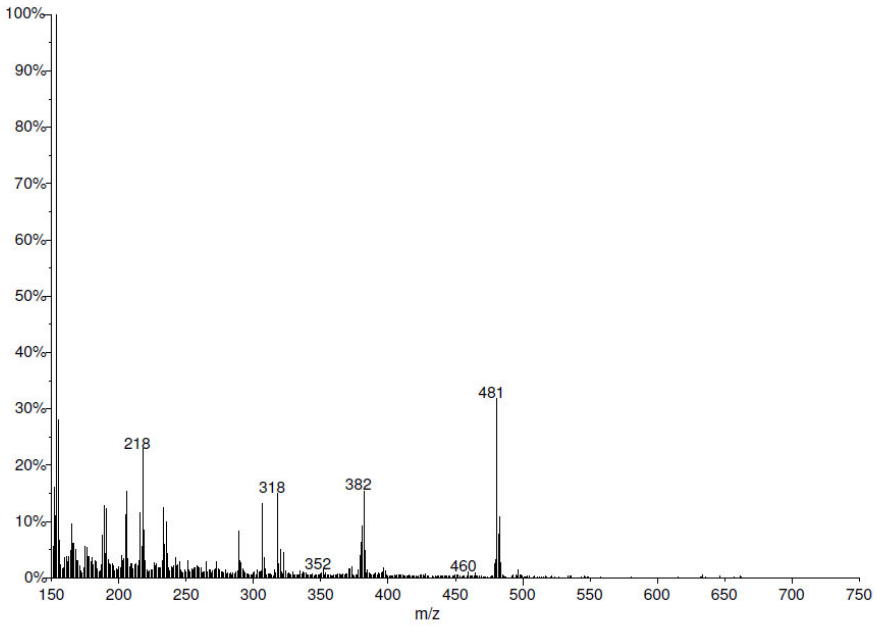

(a)

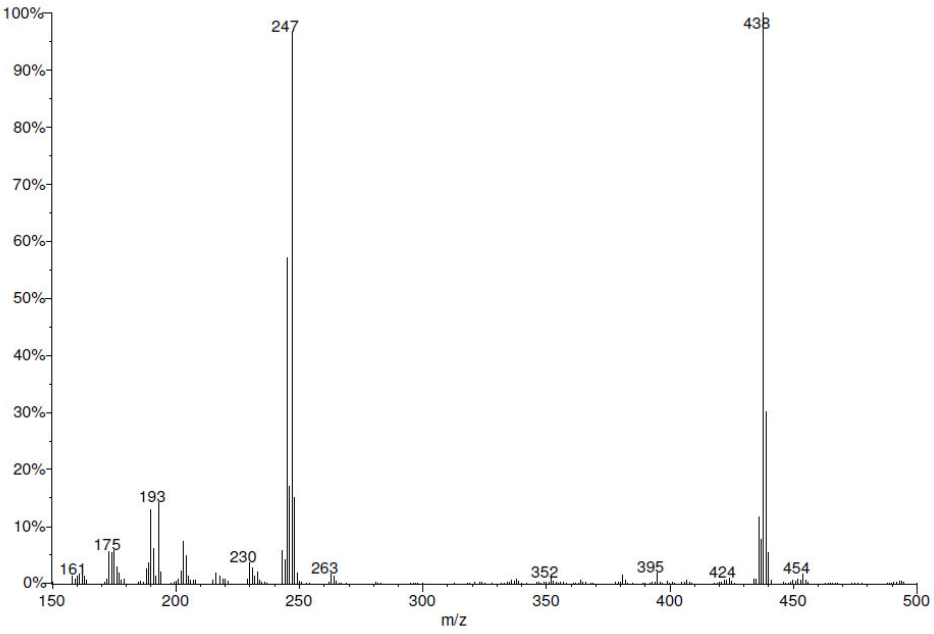

(b)

Figure S3. Positive-ion FAB mass spectra of (a) $[Fe(apHen)_2](ClO_4)_2$ and (b) $[Fe(hapMen)_2]ClO_4$.

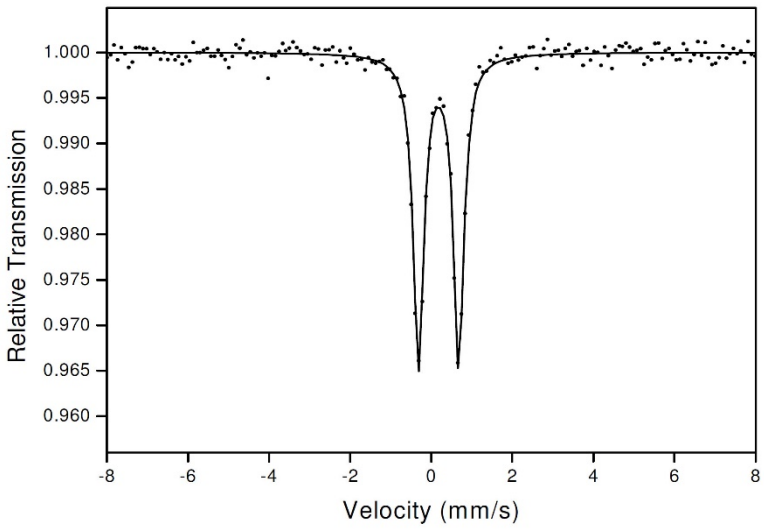

Figure S4. Mössbauer spectrum of [Fe(apMen)2](ClO4)2 at 78 K.

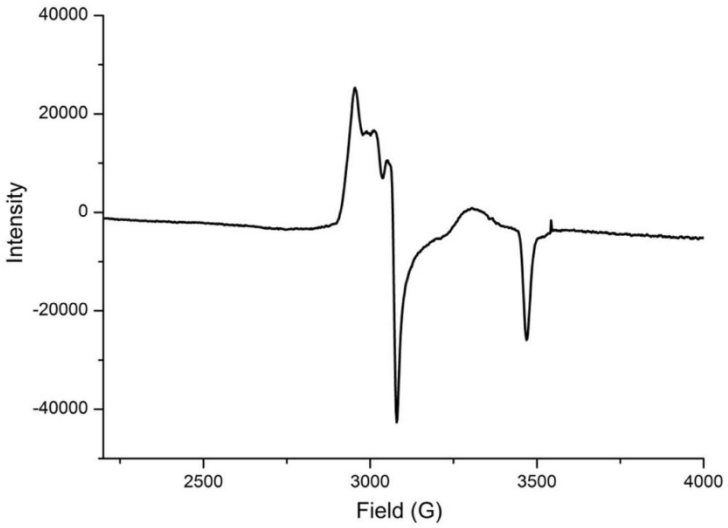

(a)

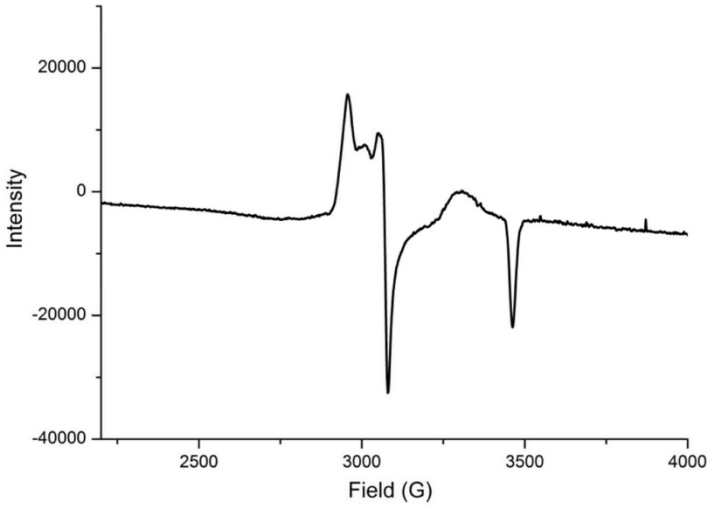

(b)

Figure S5. X-band EPR spectra of $[Fe(hapMen)_2]ClO_4$ **(a)** and $[Fe(hapEen)_2]ClO_4$ **(b)** in MeOH at 77 K.

Table S1. Selected Bond Distances (Å) and Angles (º) for [{FeIII(hapen)2}2(μ-O)]

Fe(1) Center		Fe(2) Center	
Fe(1)–O(5)	1.787(4)	Fe(2)–O(5)	1.776(5)
Fe(1)–O(2)	1.908(4)	Fe(2)–O(3)	1.912(4)
Fe(1)–O(1)	1.906(4)	Fe(2)–O(4)	1.916(5)
Fe(1)–N(1)	2.088(5)	Fe(2)–N(3)	2.090(5)
Fe(1)–N(2)	2.150(5)	Fe(2)–N(4)	2.143(5)
C(7)–N(1)	1.295(8)	C(25)–N(3)	1.290(8)
C(11)–N(2)	1.276(8)	C(29)–N(4)	1.298(8)
C(1)–O(1)	1.320(8)	C(19)–O(3)	1.316(7)
C(18)–O(2)	1.317(8)	C(36)–O(4)	1.322(8)
O(5)–Fe(1)–O(2)	112.71(19)	O(5)–Fe(2)–O(4)	113.63(19)
O(5)–Fe(1)–O(1)	109.06(19)	O(5)–Fe(2)–O(3)	108.49(19)
O(2)–Fe(1)–O(1)	92.15(19)	O(3)–Fe(2)–O(4)	92.28(19)
O(5)–Fe(1)–N(1)	104.3(2)	O(5)–Fe(2)–N(3)	104.6(2)
O(2)–Fe(1)–N(1)	141.6(2)	O(4)–Fe(2)–N(3)	140.4(2)
O(1)–Fe(1)–N(1)	85.10(19)	O(3)–Fe(2)–N(3)	84.87(19)
O(5)–Fe(1)–N(2)	103.2(2)	O(5)–Fe(2)–N(4)	102.4(2)
O(2)–Fe(1)–N(2)	84.63(19)	O(4)–Fe(2)–N(4)	84.7(2)
O(1)–Fe(1)–N(2)	146.11(19)	O(3)–Fe(2)–N(4)	147.34(19)
N(1)–Fe(1)–N(2)	77.09(19)	N(3)–Fe(1)–N(4)	77.3(2)